applied sciences

MDPI

Article

Hybrid Butterfly Optimization and Particle Swarm Optimization Algorithm-Based Constrained Multi-Objective Nonlinear Planetary Gearbox Optimization

Miloš Sedak * and Maja Rosić

Faculty of Mechanical Engineering, University of Belgrade, 11000 Belgrade, Serbia; mrosic@mas.bg.ac.rs
* Correspondence: msedak@mas.bg.ac.rs

Abstract: The multi-objective optimization (MOO) of a planetary gearbox is a challenging optimization problem, which includes simultaneous minimization of a number of conflicting objectives including gearbox volume, contact ratio, power loss, etc., and at the same time satisfying a number of complex constraints. This paper addresses this complex problem by proposing a modified hybrid algorithm, named Multi-objective Hybrid Butterfly Optimization and Particle Swarm Optimization Algorithm (HMOBPSO), which integrates PSO and Particle Swarm Optimization (BOA) algorithms with the aim to improve the performance with respect to the considered problem. The proposed approach solves the non-convex Pareto set and provides vital insights for lowering gear weight and efficiency and avoiding early failure. The experimental analysis employs numerical simulations to determine the Pareto optimal solutions to the formulated MOO problem. The results show that the proposed method offers significant improvements in terms of gearbox size, efficiency, and spacing compared to the conventional methods. In addition, an assessment of the optimization performance of the proposed HMOBPSO algorithm has been conducted by comparing it to other established algorithms across several ZDT and DTLZ benchmark problems, where it demonstrated its effectiveness.

Keywords: multi-objective optimization; planetary gear trains; gear efficiency; Particle Swarm Optimization; butterfly optimization algorithm

check for updates

Citation: Sedak, M.; Rosić, M. Hybrid Butterfly Optimization and Particle Swarm Optimization Algorithm-Based Constrained Multi-Objective Nonlinear Planetary Gearbox Optimization. *Appl. Sci.* **2023**, *13*, 11682. https://doi.org/10.3390/app132111682

Academic Editor: Marco Troncossi

Received: 11 September 2023
Revised: 1 October 2023
Accepted: 23 October 2023
Published: 25 October 2023

Copyright: © 2023 by the authors. Licensee MDPI, Basel, Switzerland. This article is an open access article distributed under the terms and conditions of the Creative Commons Attribution (CC BY) license (https://creativecommons.org/licenses/by/4.0/).

1. Introduction

Planetary gear trains are a type of mechanism that can provide high gear ratios in a compact space, and they are commonly used in various applications, including automobile transmissions, industrial drives, rotor-craft, and wind turbines [1,2]. In a planetary gear train, several planetary gears revolve around a central sun gear and a stationary central gear with internal gearing, which typically holds the entire system together. Planetary gear systems have several advantages, including their small size, high efficiency, and capacity to withstand large torque loads [1,3]. The planetary gearbox inevitably involves multiple gear mesh regions based on the number of planet branches, which, in addition to the gear material, tooth profile, lubrication, load distribution, and operating conditions, has a sizable impact on gearbox efficiency [4–6].

To improve efficiency, designers can use advanced computer simulations to predict and improve the efficiency of planetary gear systems before they are manufactured [4]. This includes optimizing the number of planetary gears and their arrangement, gear geometry, and the choice of materials and lubricants during the design stage. As a result, much research has been devoted to determining gearbox efficiency. In [5], the authors developed a computational model for predicting the mechanical efficiency of parallel-axis gear pairs and proposed a new friction coefficient model by combining a rough-surface thermal EHL model and a multiple linear regression analysis. The computational model proposed here can accurately predict the mechanical efficiency of parallel-axis gear pairs under a variety of

operating, surface, and lubrication conditions. The importance of lubrication technologies in gear transmission systems for meeting the industrial challenges of increased load, speed, and temperature is discussed in [7]. To provide more comprehensive references for gear research and engineering, the authors discuss the effects of lubrication on efficiency, fatigue performance, and dynamics. In [4], a model for calculating gear efficiency that accounts for sliding and rolling friction forces is developed, and a complete planetary gearbox's appropriate efficiency is also presented. Moreover, in [6], researchers evaluated the efficiency of a planetary multiplier gearbox with helical gears using a back-to-back gearbox test rig with recirculating power and various gear oil formulations, which resulted in distinct stabilized operating temperatures and varied power loss results based on the employed oil type. For the purpose of determining how design parameters and lubricant qualities affect the performance of planetary gearboxes, a composite power loss model and design-sensitivity study were devised and applied to wind turbines [1].

Due to present-day engineering requirements, which stem from strict regulations and a highly competitive environment, which requires the successful fulfillment of a number of criteria, including power efficiency, reliability, and noise reduction, the optimization of gear parameters has become an important area of study. The primary objective is to reduce the volume (mass) of the construction and power loss while producing improved components with a longer service life. In this regard, a great deal of research has been devoted to the optimal design of gear trains, as discussed in a number of papers [8–10].

These researchers explored gear optimization using a genetic algorithm, where the module, face width, number of teeth, and profile shift coefficients were utilized as design factors; the gear pair volume served as a fitness function; and the tooth root bending strength and contact pressure calculations were employed as constraints [8]. They concluded that the design process for gearboxes can be enhanced by employing genetic algorithms to determine the optimal parameter values for gear pairs. The problem of the optimal spur gear tooth profile has been solved using a new evolutionary optimization algorithm called the adaptive mixed differential evolution, which is based on a self-adaptive approach [9]. The objectives are to equalize the maximum bending stresses and the specific sliding coefficients at contact path extremes, which were successfully solved using the proposed method. The volume minimization of a single stage planetary gearbox was considered in [11] utilizing a hybrid algorithm combining genetic and artificial immune system algorithms, with the obtained data demonstrating improved results when compared to the existing results. The study employed nine meta-heuristics to explore the optimal design of an automatic planetary gear train [10], considering nine mixed decision parameters. The findings indicate that the differential evolution algorithm exhibited superior statistical performance compared to other algorithms, while the firefly algorithm demonstrated the most favorable convergence behavior.

The aforementioned works primarily concentrate on single-objective optimization, which is insufficient for many of the demands of contemporary engineering design problems, which frequently involve multiple conflicting objectives. Therefore, there is growing interest in the development of multi-objective optimization techniques that can handle such problems effectively. In recent times, there has been an expansion of meta-heuristic algorithms that draw inspiration from nature. These algorithms encompass a range of techniques such as the genetic algorithm [12], differential evolution [13], Particle Swarm Optimization (PSO) [14], and butterfly optimization algorithm (BOA) [15], among others. These algorithms have predominantly been designed for the purpose of solving single-objective optimization problems and have been extensively utilized in several domains, including but not limited to network configurations, telecommunications, and engineering design [8,12,13]. Nevertheless, as meta-heuristic methods continued to advance, they were also expanded to be applicable to multi-objective scenarios. This expansion gave rise to algorithms such as Non-Dominated Sorting Genetic Algorithm II (NSGA-II) [16], Differential Evolution for Multi-objective Optimization (DEMO) [17], and the more recent multi-objective non-dominated advanced BOA (MONSBOA) [18]. The utilization of enhanced

meta-heuristic optimization algorithms has led to the rise in the popularity and effectiveness of multi-objective optimization (MOO) as a viable method for addressing complex problems across diverse domains, including engineering, finance, and economics [19,20]. In engineering design, to reduce the structure volume and transmission power loss and to disclose the influence of the profile shift factor on the optimal structure fitness, researchers performed a multi-objective optimization of a corrected spur gear pair with objectives including volume, center distance, and efficiency, while contact stress, bending stress, face coefficient, and tooth-tip interference served as constraints [21]. The results reveal that the structural design is compact compared to typical ones and that it has a decent efficiency for a medium contact ratio. Researchers considered the multi-objective optimization of a two-stage helical gearbox with a wide range of constraints introduced into the optimization problem, such as bending stress, pitting stress, and tribological constraints [22]. To minimize these objective functions for three distinct gear profiles, four varieties of ISO oil grades, and two speeds, a specially formulated discrete version of the NSGA-II was implemented. The obtained results show that there is a high probability of wear failure, but when using the multi-objective approach, the total power loss of the gearbox is reduced by half. In order to reduce the weight, improve the efficiency, and prevent premature failures in planetary gearboxes, the authors developed a novel multi-objective optimization of planetary gearboxes with the minimization of weight and total power loss as objective functions [23]. Three distinct gear profiles were investigated on an industrial planetary gearbox, which exhibited significant weight and power loss improvements while also being safer in scuffing. Using volume, power output, and center distance as the objectives and eight design variables, two geometric constraints, and three design constraints, a two-stage spur gearbox's multi-objective optimization problem is formulated [24], and the NSGA-II evolutionary algorithm is used to find the Pareto frontiers. Variation and sensitivity analyses reveal that module, pinion tooth number, and face-width variables have a strong influence on volume, offering vital insights for the design of compact gearboxes. Another study considered the performance of gear systems regarding the vibration and noise produced in the process of gear transmission, and the authors formulated an optimal appropriate multi-objective modification design method for helical gear [25]. The proposed model shows that it can effectively reduce vibration and noise while ensuring even load distribution on the tooth surface. In addition, the authors developed an algorithmic framework inspired by deterministic multi-objective optimization methods, which they paired with a direct-search global optimization algorithm to generate globally Pareto-optimal solutions [26]. Two tests show that the suggested method efficiently obtains answers from the global Pareto front. In [2], the researchers developed a framework for the multi-objective uncertainty optimization design of the planetary gear train used in electric vehicles, where the volume, transmission efficiency, manufacturing size, material, and load input are taken into consideration. The results of this study show that the enhanced version of NSGA-II exhibits superior convergence efficiency in comparison to the conventional NSGA-II. In [27], the authors focused on the automatic decision making of the Pareto front applied to the design of spur gears utilizing a multi-objective optimization model solved using NSGA-II algorithm, where the variables under consideration are gear module, teeth number, transmission ratio, center distance, bearing capacity coefficient, and meshing efficiency. The study utilized three distinct methods for decision making, namely Shannon Entropy, LINMAP, and TOPSIS, to calculate the optimal solution from the Pareto frontier, showing insights into the design of spur gears. In study [28], the authors outline a technique for mitigating vibration and noise levels in the gearbox of an electric bus through the utilization of a multi-objective optimization algorithm, where the optimization of gear micro-geometry is performed. The findings indicate that the improved optimization technique, which is utilized to solve this task, can efficiently and rapidly decrease the vibration and noise levels of the gearbox. In [29], the authors consider constrained multi-objective optimization for the design of spur gear pair, where L10 life is used with various tribological constraints, including micro-pitting, flank fracture, wear, scuffing, and

scoring, incorporated as constraints in the optimization problem. The study takes into account various objectives, including weight, power loss, and heat treatment duration of the gear. The CRITIC approach is utilized to determine the most optimal solution among the Pareto-optimal solutions that have been acquired via GA optimization. The study [30] employed a genetic algorithm to optimize the parameters of gear pairs with the aim of minimizing transmission volume and power losses. The findings indicate that an optimal outcome can be achieved through the utilization of a blend of lower gear modules, face width, profile shift coefficients, and number of teeth.

This paper presents a hybridization of the PSO and BOA algorithms named the Multi-objective Hybrid Butterfly Optimization and Particle Swarm Optimization Algorithm (HMOBPSO). The objective of this algorithm is to improve optimization performance in solving complex MOO problems, with a specific focus on the formulated planetary gearbox optimization presented in this study. This paper presents a hybridization approach to mitigate the limitations encountered in optimizing conventional PSO and BOA. Specifically, the proposed method incorporates the PSO velocity update scheme into the equations governing butterfly movement. The utilization of the crowding distance has been implemented for the purpose of selecting the optimal individual within the population, with the aim of facilitating the application to multi-objective optimization problems. Moreover, the adaptive parameter has been suggested to determine the suitable expression for the individual position update in the present optimization scenario and to substitute the conventional switch probability. In summary, the findings indicate that the HMOBPSO algorithm proposed exhibits improved performance compared to the other algorithms examined with respect to both convergence rate and solution efficacy. The HMOBPSO algorithm was observed to be more efficient in discovering solutions that were characterized by greater diversity and a more uniform distribution across the Pareto front. The findings indicate that the algorithms employed were successful in enhancing the design of industrial gearboxes. Additionally, the study underscores the significance of incorporating various objectives during the design phase.

To summarize, the primary contributions of this research paper can be outlined as follows:

- This paper presents a modified methodology for optimizing the single-stage planetary gearbox through the use of MOO. The methodology takes into account a multitude of conflicting objective functions and formulates critical design constraints.
- A new optimization method, HMOBPSO, a hybrid between the PSO and BOA algorithms, has been proposed, which improves optimization performance, especially for complicated multi-objective optimization problems. Hybridization has been performed by introducing velocity-updating expression pieces from the PSO algorithm into BOA's butterfly position update equation.
- The proposed HMOBPSO algorithm was tested against NSGA-II and several other well-known algorithms in the literature on ZDT and DTLZ benchmark MOO problems. The HMOBPSO algorithm outperformed other algorithms in terms of convergence and Pareto solution quality.

The present paper is structured in the following manner. In Section 2, the formulation of the multi-objective planetary gear-optimization problem is given. Additionally, Section 2.1 presents the establishment of suitable objectives for the optimization problem regarding the planetary gearbox under consideration. The formulation of constraints is explained in Section 2.2. Section 3 presents the formulation of a multi-objective optimization problem. The theoretical underpinnings of the PSO and BOA algorithms are outlined in Sections 3.1 and 3.2, respectively. The hybridization procedure and the relevant theoretical foundations of the proposed hybrid HMOBPSO algorithm are laid out in Section 3.3. Section 4 provides an overview of the results derived from numerical experiments conducted on planetary gearbox optimization, as well as on the DTLZ and ZDT benchmark problems. Ultimately, the findings are summed up and presented in Section 5.

2. Problem Formulation

The development of planetary gearboxes that are both reliable and lightweight while maintaining high efficiency is a significant challenge in the present field of mechanical engineering. The creation of a multi-objective optimization model that integrates design variables, objectives, and constraints is crucial for attaining the intended performance of planetary gearboxes. The objective of this paper is to develop the appropriate multi-objective optimization model of a planetary gearbox and investigate the possibilities for solving this complex optimization problem, with the aim of identifying gear design parameters that can lead to weight reduction, decreased power loss, and improved reliability of components. In this context, we examine a single-stage planetary gearbox, schematically illustrated in Figure 1. The planetary gearbox under consideration comprises three planet gears and two central gears. One of the central gears features external gearing and is referred to as the sun gear, which is directly linked to the input shaft. The other central gear has internal gearing and is stationary, serving to secure the entire assembly in position. The system under consideration receives power through the input shaft and sun gear, which is subsequently distributed among the planet gears and transmitted to the carrier. The output shaft is connected to the carrier to complete the transfer of power. The analysis maintains a constant input speed of n_a = 2750 min^{-1} and a power of P_a = 175 kW throughout. The remainder of the parameters used in the design of the planetary gearbox are given in Table 1.

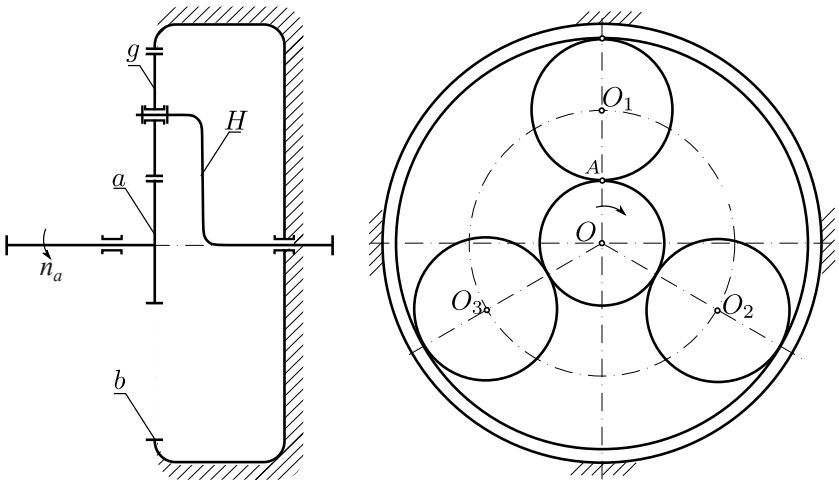

Figure 1. Schematic illustration of the planetary gearbox.

Table 1. Parameters of the planetary gearbox considered in the paper.

Parameters	Units	Symbol	Value
Input Power	kW	P_a	175
Input speed	min^{-1}	n_a	2750
Pressure angle	°	α_n	20
Gear material		*18CrNi8*	
Gear surface Roughness	µm	R_a	0.8
Factor of safety against bending	-	$S_{F\min}$	1.2
Factor of safety against pitting	-	$S_{H\min}$	1.25
Number of planet gears	-	n_w	3

The multi-objective optimization implies the simultaneous optimization of multiple objectives $f_1, f_2, \ldots, f_M$, which are often conflicting in nature. This type of optimization problem often arises in different fields of engineering, since a number of these problems involve multiple objectives and a number of constraints that need to be satisfied to ensure the physical feasibility of the solution. In general, the multi-objective optimization problem can be stated as

$$\begin{aligned} &\min f_m(\mathbf{x}_i) \quad m = 1, \ldots, M \wedge i = 1, \ldots N_P \\ &s.t. \\ &\quad g_k(\mathbf{x}_i) \geq 0, \quad k = 1, \ldots, K \\ &\quad h_l(\mathbf{x}_i) = 0, \quad l = 1, \ldots, L \\ &\quad x_{i,j} \in \left[x_j^{Lower}, x_j^{Upper}\right], \quad j = 1, \ldots, n \end{aligned} \tag{1}$$

where M is the number of objectives taken for optimization; $M \geq 2$, $g_k(\mathbf{x}_i)$ denotes the inequality constraint, with the K being the total number of inequality constraints in the considered problem; $h_l(\mathbf{x}_i)$ denotes the equality constraint, where L is the total number of equality constraints; and N_P is the number of solutions in the population. Here, the boundaries of decision variables are denoted as $x_j^{Lower}$and x_j^{Upper}.

Therefore, in formulating the MOO problem of planetary gear optimization, we start firstly with objective functions that will be taken into account, and then we present a number of constraints that are developed in order to provide a planetary gearbox with long service life.

2.1. Objectives

In this subsection, we will outline the objective functions that have been formulated for the MOO optimization problem.

2.1.1. The Volume of the Gears

Under the assumption that the density of the material is constant and that each gear is made of the same material given in Table 1, the minimization of gearbox mass can be reduced to the minimization of the volume of the gears, given as

$$f_1 = V(x) = \frac{\pi}{4} b \left[{d_{(a)}}^2 + n_w \left(d_{a(b)}^2 - D^2 \right) + \left(d_{(g)}^2 - d_s^2 \right) \right]. \tag{2}$$

2.1.2. Contact Ratio

In order to ensure smooth, continuous action between gears, it has been included as the objective as follows:

$$f_2 = \varepsilon_\alpha = \frac{0.5 \left(\sqrt{d_{a(a)}^2 - d_{a(b)}^2} + \sqrt{d_{a(g)}^2 - d_{a_g(g)}^2} \right) - a \sin \alpha_{wt}}{\pi m_t \cos \alpha_t}. \tag{3}$$

2.1.3. Safety against Bending for Central Gears

In order to ensure the normal working of gears while minimizing the dimensions, the following objectives are taken into account, which reflect the bending stress for the sun gear, which is determined based on the following equation

$$f_3 = \sigma_F = \frac{F_t}{b m_n} Y_{F_a} Y_{S_a} Y_\varepsilon K_A K_v K_{F\alpha}. \tag{4}$$

Here, the appropriate safety against the bending, which is used as a constraint in optimization, is calculated as

$$S_F(x) = \frac{[\sigma_F]_M}{\sigma_F}, \tag{5}$$

where the critical root stress, determined via the gear material, is obtained as

$$[\sigma_F]_M = \sigma_{F\,\mathrm{lim}} Y_{ST} Y_{RrelT}. \tag{6}$$

In this case, the safety factor against breaking must satisfy the following condition:

$$S_F = \frac{[\sigma_F]_M}{\sigma_F} \geq S_{F\min}, \tag{7}$$

where the S_{Fmin} is the smallest allowable safety factor value. The factors $Y_{F_a}, Y_{S_a}, Y_\varepsilon, K_A, K_v$, and $K_F\alpha$ are determined according to the ISO standard in Appendix A.

2.1.4. Safety Factor for Contact Stress

Contact stress is considered as another objective and calculated as follows:

$$f_4 = \sigma_H = Z_H Z_E Z_\varepsilon \sqrt{\frac{F_t}{bd_{(a)}} \frac{u+1}{u} K_A K_v K_{H\alpha}}, \tag{8}$$

where the appropriate safety for contact stress is determined as

$$S_H = \frac{[\sigma_H]_M}{\sigma_H}, \tag{9}$$

where the contact stress for the sun-gear–planet-gear pair is obtained as the minimum value, according to

$$\sigma_H = \min\left\{\sigma_{H,(a)}, \sigma_{H,(g)}\right\}, \tag{10}$$

where the $\sigma_{H,(a)}, \sigma_{H,(g)}$ represent the contact stress calculated for central sun gear and planet gear, respectively. The critical contact stress is determined as

$$[\sigma_H]_M = \sigma_{H\lim} Z_N Z_L Z_R, \tag{11}$$

while the safety factor from the pitting must satisfy the following condition, taken as a constraint in optimization, as follows

$$S_H = \frac{[\sigma_H]}{\sigma_H} \geq S_{H\lim}, \tag{12}$$

where the S_{Hmin} is the minimum allowed safety factor value, which is given in Table 1. The different factors used in the above equations are given in Appendix A.

2.1.5. Gearbox Efficiency

To analyze the performance of the planetary gearbox, various metrics can be employed, such as efficiency, torque, and speed ratios. The efficiency of the gearbox is defined as the ratio of output power to input power, and it is a crucial factor in determining the overall performance of the system. To calculate the efficiency of the single-gear pair in contact, we can use the model [4], which takes into account the sliding and rolling friction. Therefore, the total efficiency of a gear pair in contact can be calculated by integrating the instantaneous efficiency along the active line of action as follows:

$$\eta_{gb}^H = \frac{1}{l_a} \int_A^D \eta_i(\xi) d\xi, \tag{13}$$

where the instantaneous efficiency is determined using the numerical procedure described in [4] and calculated as

$$\eta_i(\xi) = \frac{T_2}{T_1} \frac{1}{u_{gb}^H}, \tag{14}$$

where T_1 and T_2 are the unknown torques acting on the pinion and driven gears, respectively, and u_{gb}^H is the relative gear ratio of the considered gear pair, $l_a = \overline{A_2 E_2}$ is the active length of the path of contact, ξ represents the coordinate in the coordinate system fixed with

a line of action (LOA). Using the same procedure, the efficiency η_{ag}^{H} between the central and planet gears can be calculated.

Since the planetary gearbox in Figure 1 has multiple interactions between gears in the system, in calculating the total efficiency of the complete gearbox, we start with the analysis of power flow. From the problem statement and Figure 1, it follows that the power is inputted from the central sun gear and exits from the gearbox through the shaft, which is connected to the planet carrier, while the central internal gear is stationary. Therefore, the total efficiency is

$$\eta_{aH}^{b} = \frac{P_{out}}{P_{in}} = 1 - \frac{P_{loss}}{P_{in}}, \tag{15}$$

where P_{out} is the output power captured at the exit shaft, and P_{in} is the input power at the sun gear, while P_{loss} is the total power loss, which can be calculated from the analysis of the relative efficiency η_{ab}^{H}, according to the expression

$$P_{loss} = \left(1 - \eta_{ab}^{H}\right) T_a \omega_{a,rel}, \tag{16}$$

where the $\omega_{a,rel}$ is the relative angular speed of the central gear. Substituting (16) into the (15) and taking into consideration that the angular speed ratio is

$$\frac{\omega_{a,rel}}{\omega_a} = \frac{\omega_a - \omega_H}{\omega_a} = 1 - \frac{\omega_H}{\omega_a} = 1 - \frac{1}{u_{aH}^{b}} = \frac{u_{ab}^{H}}{u_{ab}^{H} - 1}, \tag{17}$$

where ω_a is the absolute angular speed of the central gear, ω_H is the absolute angular speed of the gear carrier, and the relationship in overall gear ratio u_{aH}^{b} is $u_{aH}^{b} = 1 - u_{ab}^{H}$. Finally, we obtain the absolute efficiency of the considered planetary gearbox, which can be taken as f_5 as follows:

$$\eta_{aH}^{b} = \frac{1 - \eta_{ag}^{H}\eta_{gb}^{H}u_{ab}^{H}}{1 - u_{ab}^{H}}. \tag{18}$$

2.2. Constraints Formulation

In this section, several design constraints regarding the strength requirements employed in the MOO problem considered in this paper are outlined. Among others, the employed constraints include bending strength, pitting strength, assembly condition, etc. By implementing these constraints, the requirement for the gearbox with enhanced service life of the components is successfully satisfied.

2.2.1. Bending Constraints

The constraint regarding the gear tooth's bending strength is defined as

$$g_1 = \frac{[\sigma_F]_M}{\sigma_F} - S_{Fmin} > 0. \tag{19}$$

2.2.2. Pitting Constraints

The constraint against surface fatigue resistance has been defined as

$$g_2 = \frac{[\sigma_H]_M}{\sigma_H} - S_{Hmin} > 0. \tag{20}$$

2.2.3. Space Requirement

The mounting of the planet gears in the gearbox assembly demands the appropriate clearance between the tip circles of gears in mesh to exist. Therefore, the following constraint needs to be satisfied

$$g_3 = 2a_{ag}\sin\left(\frac{\pi}{n_w}\right) - f_z - d_{a(g)} \geq 0, \tag{21}$$

where $f_z = 0.5 \cdot m_n$ is the minimum clearance.

2.2.4. Assembly Condition

To avoid possible interference of teeth during the meshing process, the condition that must be satisfied is that the simultaneous meshing of central sun gear with planet gears must always be satisfied. In this regard, the equality constraint is defined as

$$h_1 = \frac{z_a + z_b}{n_w} - i = 0, \tag{22}$$

where i is the integer that leads to the constraint being zero.

2.3. Uniform Wear of the Teeth

The profile of the gear teeth wears down during operation, changing the size and shape of the teeth. As a result, several undesired phenomena, including vibrations and noise, happen during the transmission. Achieving uniform wear of the tooth profile of the coupled gear pair requires achieving the equality of the specific sliding in the locations that are furthest from the present pole of the relative speeds. Hence, it is imperative to examine the kinematic aspect of the coupling of gear pairs with internal and external gearing to derive the expressions for specific sliding.

Given the sliding speed, the specific sliding of the profile of the teeth of coupled gears can be defined as the ratio of the intensity of the sliding speed of the observed pair of teeth $v_{sliding,1-2}$ to the intensity of the relative speed $v_{rel,M}$ as follows

$$\nu_M = \frac{v_{sliding,1-2}}{v_{rel,M}} = \frac{v_{rel,2}}{v_{rel,1}} - 1, \tag{23}$$

where $v_{rel,i}$, $i = 1, 2$ denotes the relative speed of the driving and driven gear, respectively, at any point along the LOA. The relative speed of points M_1 and M_2, which belong to the respective profiles of the pinion and driven gear, can be determined as

$$\begin{aligned} v_{rel,M_1} &= v_{M_1}\tan\alpha_{M_1}, \\ v_{rel,M_2} &= v_{M_2}\tan\alpha_{M_2}, \end{aligned} \tag{24}$$

where the respective angles α_{M_1} and α_{M_2} can be determined from

$$\begin{aligned} \tan\alpha_{M_1} &= \frac{\rho_{M_1}}{r_{b1}}, \\ \tan\alpha_{M_2} &= \frac{\rho_{M_2}}{r_{b2}}, \end{aligned} \tag{25}$$

where the ρ_{M_1} and ρ_{M_2} are corresponding curve radii on the tooth profile of pinion and driven gear. Substituting into (23), we obtain the expression for determining the specific sliding on the pinion and driven gear

$$\begin{aligned} \nu_{M_1} &= -1 + \frac{\rho_{M_2}}{u\rho_{M_1}}, \\ \nu_{M_2} &= u\frac{\rho_{M_1}}{\rho_{M_2}} - 1, \end{aligned} \tag{26}$$

where u is the gear ratio of the considered gear pair. Since the specific sliding on the gear profile is highest on the points furthest from pole C, determining the specific sliding in points A_1 and E_2 with equations

$$\begin{aligned} \nu_{A_1} &= \frac{\rho_{E_2}}{u\rho_{A_1}} - 1, \\ \nu_{A_2} &= u\frac{\rho_{E_1}}{\rho_{A_2}} - 1, \end{aligned} \tag{27}$$

is of interest, where the ρ_{A_1}, ρ_{E_1} and ρ_{A_2}, ρ_{E_2} are corresponding curve radii on the tooth profile of the pinion and driven gear. In order to analyze the specific sliding in the characteristic points on the involute profile of the gears in coupling, Figure 2 shows the dependence of the specific sliding of simultaneously coupled teeth, for a gear pair with the parameters: $z_1 = 20$, $z_2 = 100$, $m_n = 3$ mm, $x_1 = x_2 = 0$, $\alpha = 20°$.

Based on the geometric interpretation of the obtained results, in Figure 2, it follows that the value of specific sliding is the largest at the beginning of the meshing at the base of the profile of the pinion E_1 and the top of the profile of the tooth of the driven gear A_2. In the kinematic pole (point C) the specific sliding is equal to zero. When the coupled profiles pass through pole C, the sliding speeds change direction to the corresponding points on the top of the pinion and the base E_2 of the driven gear. Therefore, it is of interest to analyze how to modify the value of specific sliding. Therefore, in Figure 3, we presented the sensitivity analysis of the maximum value of specific sliding on the pinion and driven gear as a function of profile shift coefficients.

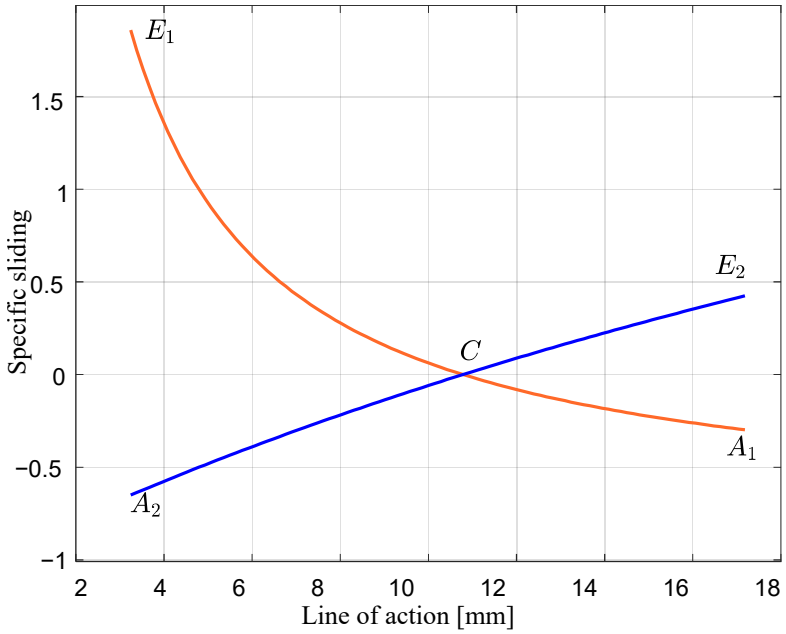

Figure 2. Specific sliding at different points on the pinion and driven gear along the line of action.

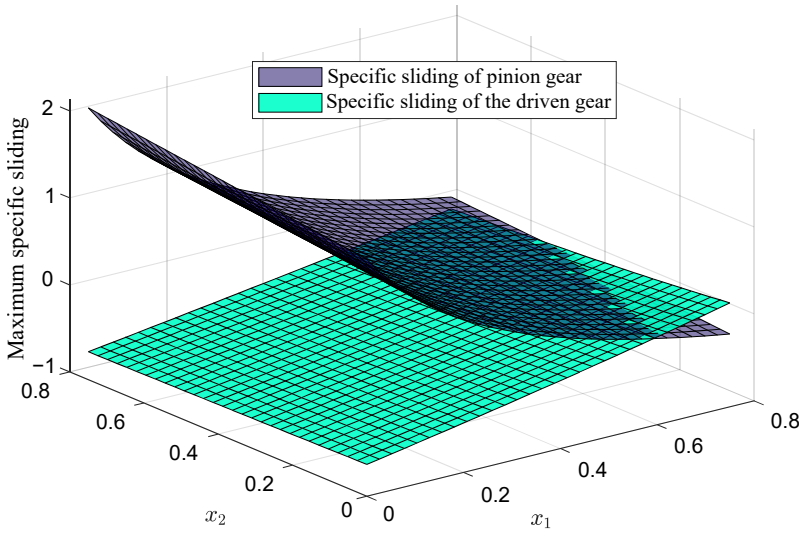

Figure 3. Maximum value of the specific sliding of pinion and driven gear as a function of profile shift coefficients x_1 and x_2.

From Figure 3, we observe that it is possible to change the value of specific sliding with the appropriate changes in profile shift coefficients. Based on this analysis, it follows that setting a constraint in the MOO model in the form of equality of specific sliding at the top and bottom of the profile of the coupled teeth is necessary in order to ensure the uniformity of wear of the coupled gears profiles. Furthermore, this shows the necessity of introducing the profile shift coefficients as design variables in optimization.

Design Variables

In this paper, a total of seven design variables are considered during the optimization, including z_a, the number of teeth of the central gear; z_b, the number of teeth of the central stationary gear with internal gearing; z_g, the number of teeth of the planetary gear; m, the module of gears in the gearbox; and x_a, x_b, and x_g, the profile shift coefficients of the central, internal, and planet gears, respectively. The design vector is therefore

$$\mathbf{x} = \left[z_a, z_b, z_g, m, x_a, x_b, x_g\right]^T. \tag{28}$$

In Table 2 we have given the specification of design variables as well as the types of variable and their bound range.

Table 2. Details of the design variables.

Design Variable	Lower Bound	Upper Bound	Type
z_a	17	26	Integer
z_b	22	60	Integer
z_g	40	120	Integer
m	2	40	Discrete
x_a	-0.5	1	Continuous
x_b	-0.5	1	Continuous
x_g	0.0	0.5	Continuous

3. Multi-Objective Optimization

3.1. Multi-Objective Particle Swarm Optimization Algorithm

The PSO belongs to a group of nature-inspired evolutionary algorithms (EAs), whose mechanisms are inspired by bird-swarming behavior in the process of searching for food [14]. The optimization process of the PSO algorithm starts with the creation of the swarm of N_P particles in the swarm, written as the set $P^{(G)} = \{\mathbf{x}_i \mid \mathbf{x}_i \in \mathbb{F}\}$, $i \in \{1, 2, \ldots, N_P\}$, where $\mathbb{F}$ denotes the feasible solution space, and G is the current generation index in the initial generation $G = 0$. The current position $\mathbf{x}_i^{(G)}$ of each particle is influenced by the appropriate speed vector $\mathbf{s}_i^{(G)}$. The vector $\mathbf{s}_i^{(G)}$ is thus influenced by the best position that each particle has previously discovered, denoted as $\mathbf{x}_{pbest,i}^{(G)}$, and the best position discovered by the entire swarm of particles $\mathbf{x}_{gbest}^{(G)}$. These parameters represent particles' individual intelligence and the group swarm's intelligence. In each generation, the position of particles is changed according to

$$\mathbf{s}_i^{(G+1)} = \mathbf{s}_i^{(G)} + c_1 rand_1 \left(\mathbf{x}_{pbest,i}^{(G)} - \mathbf{x}_i^{(G)}\right) + c_2 rand_2 \left(\mathbf{x}_{gbest}^{(G)} - \mathbf{x}_i^{(G)}\right), \tag{29}$$

$$\mathbf{x}_i^{(G+1)} = \mathbf{x}_i^{(G)} + \mathbf{s}_i^{(G+1)}, \tag{30}$$

where c_1 represents the cognitive and c_2 social coefficients, and $rand_1$ and $rand_2$ are random numbers in the range $rand_i \in (0, 1)$, $i = 1, 2$, such that $rand_1 \neq rand_2$. To update the personal best position discovered by each particle in each generation in application to multi-objective optimization, we modify the original PSO in a way that the modification of

the personal best position of each particle occurs when the present personal best solution is dominated by the current position, as expressed by the subsequent equation

$$\mathbf{x}_{pbest,i}^{(G+1)} = \begin{cases} \mathbf{x}_{pbest,i}^{(G)}, & \text{if } \mathbf{x}_{pbest,i}^{(G)} \prec \mathbf{x}_{i}^{(G)} \\ \mathbf{x}_{i}^{(G)}, & \text{otherwise} \end{cases}. \tag{31}$$

To update the global best position $\mathbf{x}_{gbest}^{(G)}$ due to the conflicting nature of the objectives in a multi-objective optimization problem, and when there is no single solution to be used, an external archive is employed. In this archive, a set of non-dominated solutions obtained in the optimization process is memorized. Then, in each generation, the crowding distance is employed to evaluate the diversity of solutions in the archive, and the solution $\mathbf{x}_{gbest}^{(G)}$ is selected using the binary tournament [31,32].

3.2. Butterfly Optimization Algorithm

BOA is a novel meta-heuristic optimization technique that was developed by Arora and Singh [15] in 2010 and has gained popularity due to its ability to solve complex optimization problems in various fields. The BOA algorithm is based on the behavior of butterflies in their search for food and mates. The BOA algorithm mimics the biological system and the behavior of butterflies by creating a population of solutions that are updated and improved over time through a series of iterations, and it is based on the following assumptions:

1. Every butterfly releases a fragrance that draws other butterflies to it.
2. Butterflies either fly randomly or deliberately toward the butterfly that gives off the strongest fragrance.
3. The objective function value of the butterfly under consideration determines the strength of the butterfly stimulus.

During the optimization process, the BOA algorithm goes through three phases. Firstly, in the initialization stage, all parameters of the algorithm are set, and the initial population is randomly generated within the bounds of solution feasibility. Next, the iteration stage is repeated until the algorithm converges toward the optimal solution, at which point BOA performs the search for the global optimal solution. Finally, at the optimization stage, the optimal solution is obtained and presented. The iteration stage is performed such that the objective function is evaluated for each butterfly in the population, and based on this value, a fragrance is created. Therefore, the stimulus intensity, denoted as I, for the ith butterfly can be determined as

$$I = f\left(\mathbf{x}_{i}^{(G)}\right), \tag{32}$$

where $\mathbf{x}_i$ is the ith butterfly in the population and $f(\cdot)$ denotes the objective function. Each firefly senses the fragrance, and the degree of the fragrance sensed by the butterfly, designated as φ_i, can be determined as a function of I as follows:

$$\varphi_i = cI^a, \tag{33}$$

where a denotes the power exponent and c is the sensory fragrance parameter such that $c \in [0, 1]$. Regarding the parameter a, when $a = 0$, other butterflies are unable to smell any butterfly's scent, but there is no fragrance absorption when $a = 1$.

The movement of each butterfly in the population is decided based on the switch probability p; in this regard, either a global or local search is performed. The global search phase is performed according to the expression

$$\mathbf{x}_{i}^{(G+1)} = \mathbf{x}_{i}^{(G)} + \left(r^2 \times \mathbf{g}^* - \mathbf{x}_{i}^{(G)}\right) \times \varphi_i, \tag{34}$$

where $\mathbf{g}^*$ denotes the butterfly that emitted the strongest fragrance, i.e., achieved the best objective function value, and $r \in [0,1]$ is a uniformly generated random number. The local search is performed using the expression

$$\mathbf{x}_i^{(G+1)} = \mathbf{x}_i^{(G)} + \left(r^2 \times \mathbf{x}_j^{(G)} - \mathbf{x}_k^{(G)}\right) \times \varphi_i, \tag{35}$$

where $\mathbf{x}_j^{(G)}$ and $\mathbf{x}_k^{(G)}$ are the jth and kth butterflies chosen randomly from the solution space. Thus, the movement of the ith butterfly is described as

$$\mathbf{x}_i^{(G+1)} = \begin{cases} \mathbf{x}_i^{(G)} + \left(r^2 \times \mathbf{g}^* - \mathbf{x}_i^{(G)}\right) \times \varphi_i, & \text{for } r_p < p \\ \mathbf{x}_i^{(G)} + \left(r^2 \times \mathbf{x}_j^{(G)} - \mathbf{x}_k^{(G)}\right) \times \varphi_i, & \text{otherwise} \end{cases} \tag{36}$$

where we see that the global search is activated if the randomly generated number r_p is less than p; otherwise, a local search is performed. The iteration stage is repeated until the algorithm converges and the solution is displayed.

3.3. Multi-Objective Hybrid Butterfly Optimization and Particle Swarm Optimization Algorithm

Due to the inherent conflicting nature of objective functions in multi-objective optimization problems, there is no single solution that simultaneously minimizes all considered objective functions. Therefore, in solving MOO problems, it is crucial to obtain a set of solutions, called Pareto-optimal solutions (Pareto front), which are considered optimal because they represent a trade-off between the objectives, meaning that improving one objective comes at the cost of worsening another. The acquired Pareto set offers decision makers a variety of possibilities from which to pick based on their preferences and priorities. Let us consider the MOO problem in Equation (1); then, the feasible domain $\mathbb{F}$ is a set of solutions that satisfy all the constraints imposed on the considered problem, which is written as

$$\mathbb{F} = \left\{ \mathbf{x} \mid g_k(\mathbf{x}_i) \geq 0 \wedge h_l(\mathbf{x}_i) = 0 \wedge x_{i,j} \in \left[x_j^{Lower}, x_j^{Upper}\right] \right\} \tag{37}$$

Then, for each solution $\mathbf{x} \in \mathbb{F}$, we say that it is Pareto-optimal if and only if there does not exist any point $\mathbf{y} \in \mathbb{F}$ for which $f(\mathbf{y}) \leq f(\mathbf{x})$, such that $f(\mathbf{y}) \neq f(\mathbf{x})$.

Definition 1. *Non-dominated solution: The solution* $\mathbf{x}$ *is said to be non-dominated (or Pareto-optimal) if and only if there does not exist another solution* $\mathbf{y}$ *such that* $f_i(\mathbf{x}) \leq f_i(\mathbf{y})$, $\forall i \in \{1, 2, \ldots, M\}$ *with at least one strict inequality, i.e.,* $\exists j \in \{1, 2, \ldots, M\} : f_j(\mathbf{x}) < f_j(\mathbf{y})$

Definition 2. *Pareto front: The set, which is composed of non-dominated Pareto-optimal solutions, is called the Pareto front (PF), denoted as* $X = \{\, \mathbf{x} \in \mathbb{F} | \nexists \mathbf{y} \in \mathbb{F}$ *, such that* $f(\mathbf{y}) > f(\mathbf{x}) \,\}$.

The BOA and PSO algorithms, however, were both initially proposed for single-objective optimization problems. Later, different versions of the PSO algorithm for MOO problems, as well as, in recent years, the BOA algorithm, were developed [18]. Furthermore, to successfully solve MOO problems, we need to provide an adequate balance between exploration and exploitation and keep population diversity. As a result, in order to successfully handle complex MOO problems, the proposed multi-objective Hybrid Butterfly Optimization and Particle Swarm Optimization Algorithm, named HMOBPSO, aims to discover the Pareto optimal of the considered problem. This is accomplished by introducing a selection operator based on crowding distance, as well as a separate archive in which all non-dominated solutions found in each iteration are saved. Furthermore, with the introduction of the appropriate hybridization between BOA and PSO algorithms, which utilizes the adaptive parameter in determining which strategy to apply to the current optimization stage, the algorithm effectively maintains the population diversity. By incorporating a hybrid approach, the algorithm is able to overcome the limitations of each individual

method and achieve better performance in solving complex multi-objective optimization problems.

Firstly, the selection strategy, based on the crowding distance, is used to select the solutions that will be kept in the archive $\mathbb{P}_s$. The crowding distance is a measure of how crowded a solution is in the objective space. Solutions that are too close to each other are considered redundant and only one of them needs to be kept in the archive. The selection strategy ensures that the archive contains a diverse set of non-dominated solutions that cover the entire objective space. In each iteration, we compare all solutions written to the archive $\mathbb{P}_s$ in order to determine whether the newly obtained solution should enter the archive. Therefore, each solution is compared with each non-dominated solution in $\mathbb{P}_s$ in order to determine whether the solution should stay in the archive.

Next, by looking into the mechanisms for the updating of particle positions of both PSO and BOA algorithms, we observe that both algorithms have their strengths and weaknesses in finding the optimal solution. Therefore, to improve the global exploration ability of the proposed algorithm, we propose the integration of the term $c_2 rand_2\left(\mathbf{x}_{gbest}^{(G)} - \mathbf{x}_i^{(G)}\right)$ from the velocity-updating equation from the PSO algorithm into Equation (34) of the BOA algorithm, and, substituting the term $\mathbf{g}^*$ with $\mathbf{x}_{gbest}^{(G)}$, we obtain

$$\mathbf{x}_i^{(G+1)} = \mathbf{x}_i^{(G)} + \left(r^2 \times \mathbf{x}_{gbest}^{(G)} - \mathbf{x}_i^{(G)}\right) \times \varphi_i + c_2 rand_2\left(\mathbf{x}_{gbest}^{(G)} - \mathbf{x}_i^{(G)}\right). \tag{38}$$

On the other hand, in order to improve the exploitation ability, the term $c_1 rand_1\left(\mathbf{x}_{pbest,i}^{(G)} - \mathbf{x}_i^{(G)}\right)$ from Equation (29) has been introduced into Equation (35), and the following is obtained

$$\mathbf{x}_i^{(G+1)} = \mathbf{x}_i^{(G)} + \left(r^2 \times \mathbf{x}_j^{(G)} - \mathbf{x}_k^{(G)}\right) \times \varphi_i + c_1 rand_1\left(\mathbf{x}_{pbest,i}^{(G)} - \mathbf{x}_i^{(G)}\right), \tag{39}$$

where, due to the multi-objective nature of the problem, the term φ_i is calculated according to the following expression

$$\varphi_i = \sum_{i=1}^{M} w_i \cdot f_i, \tag{40}$$

where the set of weights w_i, $i = 1, ..., M$ is chosen randomly to satisfy the condition

$$\sum_{i=1}^{M} w_i = 1. \tag{41}$$

In order to maintain the population diversity and explore the complete Pareto set, in this paper, an adaptive parameter using the normalized population spacing is employed to regulate which developed expression will be applied, which can be calculated as

$$PS^{(G+1)} = \sqrt{\frac{1}{N_P - 1} \sum_{i=1}^{N_P} \left(\bar{d}^{(G+1)} - d_i^{(G+1)}\right)^2}, \tag{42}$$

where $d_i^{(G+1)}$ is the distance between the ith particle and other particles in the population, and $\bar{d}^{(G+1)}$ represents the average minimum distance of all particles. In this regard, a large value of this parameter indicates a diverse and spread-out population, which indicates that the global search should be intensified. On the other hand, a smaller value of this parameter indicates that the population is grouped in one region, so the local search is to be intensified.

Based on this, the appropriate pseudo-code of the proposed HMOBPSO algorithm, with the mechanism described above for updating the particle position is outlined in Algorithm 1.

Algorithm 1 Pseudo-code of the proposed hybrid butterfly optimization and Particle Swarm Optimization Algorithm—HMOBPSO.

Initialize the parameters N_P, n, a, c, c_1, c_2, $MaxIter$
Uniformly and randomly generate initial solutions $\mathbf{x}_i^{(0)} \quad \forall i = 1, 2, \ldots, N_P$
Set the initial $\mathbf{x}_{i,pbest}^{(0)}$ and $\mathbf{x}_{gbest}^{(0)}$ values
Calculate initial intensity I and φ_i
Initialize archive $\mathbb{P}_s$
while $iter < MaxIter$ **do**
  for i = 1:N_P **do**
    Calculate the adaptive parameter $PS^{(G+1)} = \sqrt{\frac{1}{N_P - 1} \sum_{i=1}^{N_P} \left(\bar{d}^{(G+1)} - d_i^{(G+1)} \right)^2}$
    if $PS^{(G+1)} > 0.5$ **then**
      $\mathbf{x}_i^{(G+1)} = \mathbf{x}_i^{(G)} + \left(r^2 \times \mathbf{x}_{gbest}^{(G)} - \mathbf{x}_i^{(G)} \right) \times \varphi_i + c_2 rand_2 \left(\mathbf{x}_{gbest}^{(G)} - \mathbf{x}_i^{(G)} \right)$
    else if $PS^{(G+1)} \leq 0.5$ **then**
      $\mathbf{x}_i^{(G+1)} = \mathbf{x}_i^{(G)} + \left(r^2 \times \mathbf{x}_j^{(G)} - \mathbf{x}_k^{(G)} \right) \times \varphi_i + c_1 rand_1 \left(\mathbf{x}_{pbest,i}^{(G)} - \mathbf{x}_i^{(G)} \right)$
    end if
    Update archive $\mathbb{P}_s$
    Determine the personal best solution according to
    $\mathbf{x}_{i,pbest}^{(G+1)} = \begin{cases} \mathbf{x}_{i,pbest}^{(G)}, & \text{if} \mathbf{x}_{i,pbest}^{(G)} \prec \mathbf{x}_i^{(G)} \\ \mathbf{x}_i^{(G)}, & \text{otherwise} \end{cases}$
    Calculate $\mathbf{x}_{gbest}^{(G)}$
  end for
end while

The methodology of the proposed HMOBPSO algorithm, described above, can be divided into the following steps:

1. *Initialize parameters:* Initialize parameters of the HMOBPSO algorithm, including the population size N_P, the maximum number of generations $MaxIter$, and the lower and upper bounds of decision space x_j^{Lower}, x_j^{Upper}. Furthermore, initialize $c_1 = 2$, $c_2 = 2$, a =0.25, c =0.01.
2. *Generate the initial population:* Generate the initial population of solutions by randomly deploying N_P solutions within the predefined bounds using the equation

$$x_{i,j}^{(o)} = x_j^{Lower} + \left(x_j^{Upper} - x_j^{Lower} \right) \cdot rand,$$

   where $rand$ is a random number in $[0, 1]$ and the vector of initial positions is $\mathbf{x}_i^{(0)} = \left[x_{i,1}^{(0)}, x_{i,2}^{(0)}, \ldots, x_{i,j}^{(0)}, \ldots, x_{i,n}^{(0)} \right], \forall i = 1, \ldots, N_P$,
3. *Calculate the objective function:* Calculate the objective function value in each $\mathbf{x}_i^{(0)}$,
4. *Initialize the global and local best:* Initialize the local best solution $\mathbf{x}_{i,pbest}^{(0)}, \forall i = 1, \ldots, N_P$, the same as the initial population $\mathbf{x}_i^{(o)}$. Based on the calculated objective function value, sort the population and determine the global best solution $\mathbf{x}_{gbest}^{(0)}$.
5. *Calculate initial intensity and fragrance:* For each $\mathbf{x}_i^{(0)}$ calculate the intensity I using the Equation (32) and fragrance φ_i using the Equation (33),
6. *Initialize the archive:* Initialize the empty archive $\mathbb{P}_s$.
7. *The following process is repeated until the stopping criterion is reached:*
8. *Calculate adaptive parameter:* PS^{G+1} Using Equation (42), calculate the value of parameter PS^{G+1}. This value will guide the process of optimization.
9. *Check the parameter* PS^{G+1} *and move the population:* Based on the value of parameter PS^{G+1}, apply the appropriate equation for the movement of population to each

$\mathbf{x}_i^{(G)}$ in the population $(i = 1, \ldots, N_P)$. Therefore, if $PS^{G+1} > 0.5$, we apply the expression shown in Equation (38), which facilitates the exploration of the solution space. Otherwise, when $PS^{G+1} \leq 0.5$, we apply the expression shown in Equation (39) to improve local search.

10. *Calculate the crowding distance:* For each newly obtained solution in the population, calculate the crowding distance.
11. *Update archive:* $\mathbb{P}_s$ Based on the calculated crowding distance, update the archive $\mathbb{P}_s$, where each solution is compared with each non-dominated solution in an archive in order to determine whether the solution should stay in the archive.
12. *Update the personal best:* Using the expression

$$\mathbf{x}_{i,pbest}^{(G+1)} = \begin{cases} \mathbf{x}_{i,pbest}^{(G)}, & \text{if} \mathbf{x}_{i,pbest}^{(G)} \prec \mathbf{x}_i^{(G)} \\ \mathbf{x}_i^{(G)}, & \text{otherwise} \end{cases},$$
$$\forall i = 1, 2, \ldots, N_P$$

update the personal best solution of the entire population.

13. *Update the global best:* Using the solutions in the archive $\mathbb{P}_s$, update the global best solution $\mathbf{x}_{gbest}^{(G)}$.
14. *Stopping criterion:* Stop the execution of the HMOBPSO algorithm if the termination criterion is satisfied and go to Step 15; otherwise, go to Step 7 and repeat the search for the global optimal solution.
15. *Display result:* Display the optimal result, which is reflected through the appropriate Pareto-optimal set as well as a set of solutions that belong to the Pareto-optimal set.

The appropriate diagram depicting the process of the optimization of the planetary gearbox using the proposed HMOBPSO algorithm is shown in Figure 4.

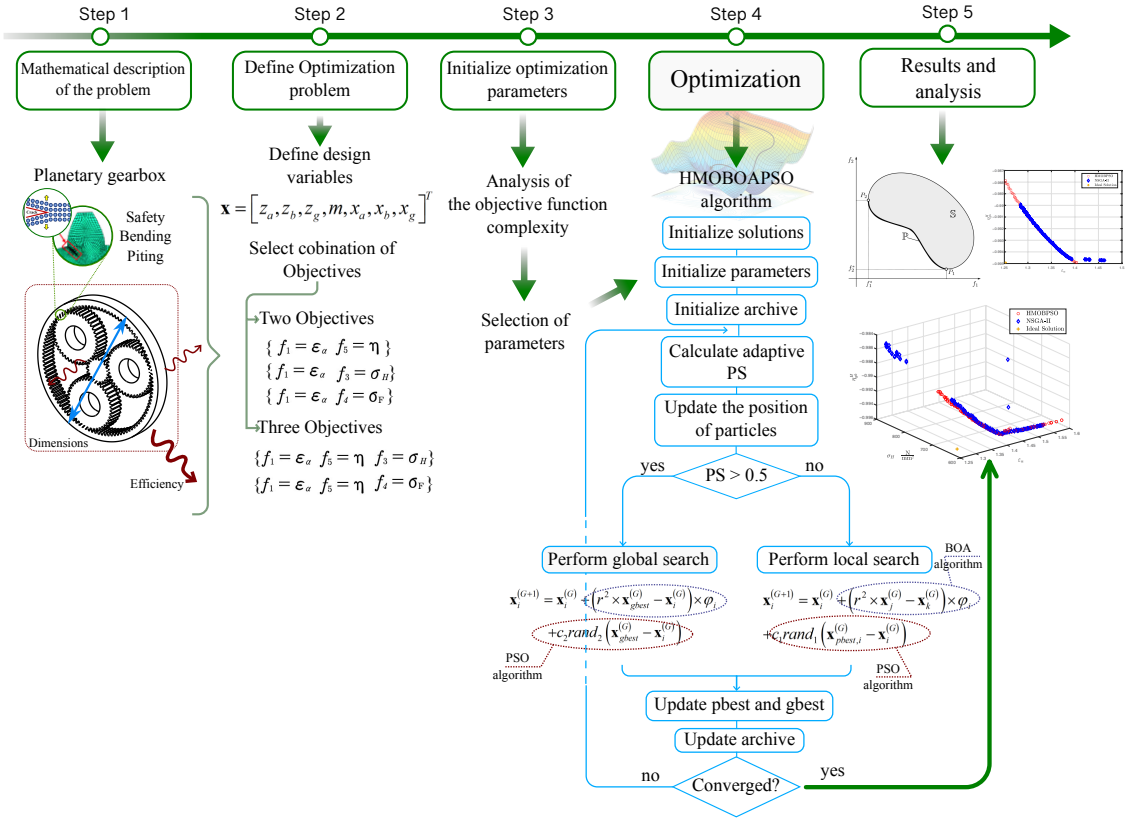

Figure 4. Graphic illustration of the application of the HMOBPSO algorithm on the planetary-gearbox-optimization problem.

4. Experimental Results

This section presents an numerical analysis of the optimization performance of the HMOBPSO algorithm. The experimental analysis employs numerical simulations to determine the Pareto-optimal solutions to the formulated MOO problem of optimizing the planetary gearbox. Furthermore, to validate the hybridization proposed in this paper, we conduct a statistical analysis to compare the optimization performance of the proposed HMOBPSO algorithm with that of several established algorithms, namely NSGA-II [16], MOPSO [33], CMOPSO [34], and MOBOA [35], on DTLZ and ZDT benchmark problems. For the analysis in this section, the parameters of the algorithms used are displayed in Table 3.

Table 3. Specification of parameters of the optimization algorithm used in numerical experiments.

Algorithm	Population Size N_P	Max. Number of Iterations	Other Relevant Parameters
HMOBPSO	100	10,000	$c_1 = 2$; $c_2 = 2$; $c = 0.01$; $a = 0.25$
NSGA-II			$p_c = 0.9$—crossover probability; $p_m = 0.33$—mutation probability; $\eta_c = 2$ crossover index
CMOPSO			$\gamma = 10$ size of elite particle set
MOPSO			Repository size = 100; Mutation rate = 0.5
MOBOA			Switch probability − 0.5

4.1. The Planetary Gear Train Optimization

Here, we present the results of numerical simulations conducted on the optimization model of the planetary gearbox defined in Section 2. For reference purposes and for comparison, the obtained gearbox parameters are compared with an example from the reference literature outlined in AGMA [36], whose parameters are shown in Table 4. Firstly, the analysis of conflicting objectives is performed, where we have concluded that the objectives gearbox volume V (Equation (2)), center distance a, and contact ratio ε_α (Equation (3)) are not conflicting objectives and that a linear relationship can be established between them, with a correlation coefficient of 0.6, as shown in the Figure 5.

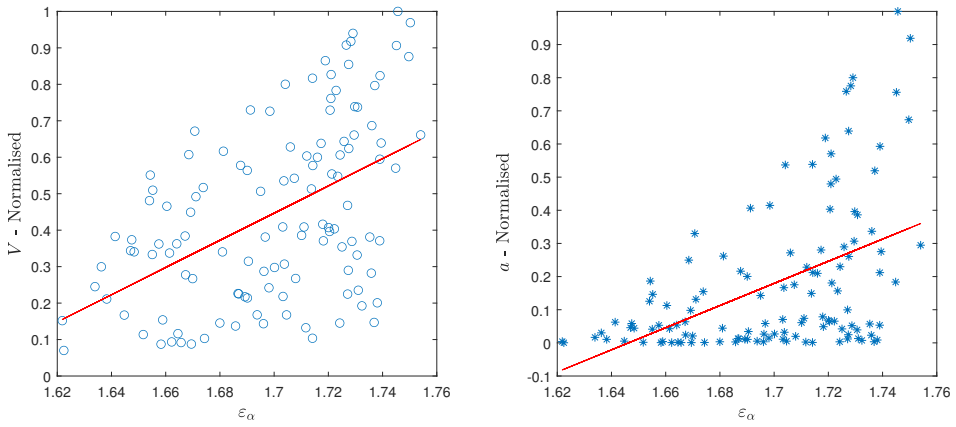

Figure 5. The non-conflicting relationship between gearbox volume V, center distance a, and contact ratio ε_α. On the figures the red line represents the fitted linear relationship.

Therefore, for the next analysis, only one of these objectives will be taken into consideration in combination with other conflicting objectives. Thus, we take into consideration several combinations of objectives, including:

- Contact ratio (defined in Equation (3)) in combination with the gearbox efficiency η_{gb}^H defined in Equation (18),
- Contact ratio ε_α with the bending stress σ_F defined in Equation (4)
- Contact ratio with the contact stress σ_H defined in (8),

as well as three objective problems, which include the following combinations:

- Contact ratio ε_α with the gearbox efficiency η_{gb}^H and bending stress σ_F, and
- Contact ratio ε_α with the gearbox efficiency η_{gb}^H and contact stress σ_H.

Table 4. Parameters of reference gearbox outlined in [36].

Parameter	Value
z_1	20
z_2	37
z_3	94
m (mm)	9
a (mm)	295.6 mm
η_{gb}^H	0.97
V (mm^3)	3.66×10^{10}
ε_α	1.36

As stated in the introduction, since the majority of papers employ the NSGA-II algorithm for engineering multi-objective optimization, we have performed numerical simulations with NSGA-II and proposed the HMOBPSO algorithm for comparison. The parameters used in the simulations are $N_P = 100$ particles and a maximum number of generations of 10,000. The remaining parameters of these optimization algorithms are displayed in Table 3. The simulations are performed using MATLAB software on a computer with 3.2 GHz CPU and 16 GB of RAM. Since the considered objectives are conflicting, there is no single solution that can be extracted; rather, a Pareto set of solutions is obtained and presented. Therefore, for comparison, an ideal solution $\mathbf{x}_{ideal} = (x_{ideal,1}, x_{ideal,2}, \ldots, x_{ideal,M})$ is firstly generated as follows:

$$x_{ideal,i} = min(f_i), \quad \forall i = 1, 2, \ldots, M \tag{43}$$

where M is the number of objectives. Since solution $\mathbf{x}_{ideal}$ does not belong to the obtained Pareto set, for the comparison, we obtained a compromise solution, as the solution closest to the Pareto front to the ideal solution, with the Euclidean distance serving as the measure of proximity.

The compromise solutions, derived through numerical simulation for various combinations of objective functions described above, are presented in Table 5. These solutions were obtained using both the proposed HMOBPSO algorithm and the widely used NSGA-II algorithm. Additionally, the values for the reference AGMA gearbox are included in Table 4 for comparison.

To achieve an in-depth understanding of the data shown in Table 5, a visual overview of the Pareto-optimal curves for the multi-objective optimization problem under consideration, which were derived using both the proposed and the NSGA-II algorithm, were analyzed. The Pareto optimum curves offer a graphical depiction of the trade-offs among several objectives, enabling decision-makers to choose the most appropriate solution according to their preferences, not just the compromise solution.

Since the gearbox efficiency and dimensions are of greatest importance, it is vital to examine the impact of variations in the contact ratio (representing the gearbox dimensions) of the planetary gearbox on the overall efficiency of the gearbox, where the appropriate Pareto curves are presented in Figure 6.

The Pareto optimum curves depicted in Figure 6 illustrate the presence of conflicting objectives. The ideal values for the contact ratio and efficiency of the gearbox are $\varepsilon_\alpha = 1.25$ and $\eta_{gb}^H = 0.9949$, correspondingly, while the compromise solution for NSGA-II is $\varepsilon_\alpha = 1.4$ and $\eta_{gb}^H = 0.9932$ and $\varepsilon_\alpha = 1.35$ and $\eta_{gb}^H = 0.9949$ for the HMOBPSO algorithm. It has been observed that the NSGA-II algorithm fails to achieve the entirety of the Pareto curve, hence omitting crucial information that is essential for the designer.

Table 5. The obtained values of design variables for the considered MOO problem of the planetary gearbox and parameters of the reference industrial gearbox.

Algorithm	z_1	z_2	z_3	m **mm**	x_1	x_2	x_3	a **mm**	η_{gb}^H	V **mm**^{3}	ε_α
Objectives ε_α and σ_F											
HMOBPSO	19	22	60	10	0.70	0.50	0.50	215.31	0.9873	3.99×10^9	1.27
NSGA-II	19	22	97	10	0.70	0.50	0.50	215.31	0.9842	1.62×10^{10}	1.27
Objectives ε_α and σ_H											
HMOBPSO	20	23	104	10	0.70	0.50	0.50	225.35	0.9914	2.28×10^{10}	1.29
NSGA-II	22	43	105	10	0.70	0.50	0.50	335.78	0.9850	7.43×10^{10}	1.40
Objectives ε_α and η_{gb}^H											
HMOBPSO	20	35	45	10	0.70	0.50	0.50	285.62	0.9949	3.76×10^9	1.35
NSGA-II	22	43	45	10	0.70	0.49	0.50	335.69	0.9933	5.99×10^9	1.40
Objectives ε_α, σ_H and η_{gb}^H											
HMOBPSO	20	23	47	10	0.69	0.50	0.50	225.28	0.9925	2.23×10^9	1.29
NSGA-II	21	28	45	10	0.70	0.50	0.50	255.51	0.9903	2.79×10^9	1.33
Objectives ε_α, σ_F and η_{gb}^H											
HMOBPSO	19	22	46	10	0.70	376.00	0.38	214.35	0.9912	1.84×10^9	1.30
NSGA-II	22	22	45	10	0.70	0.49	0.50	230.32	0.9894	2.12×10^9	1.31

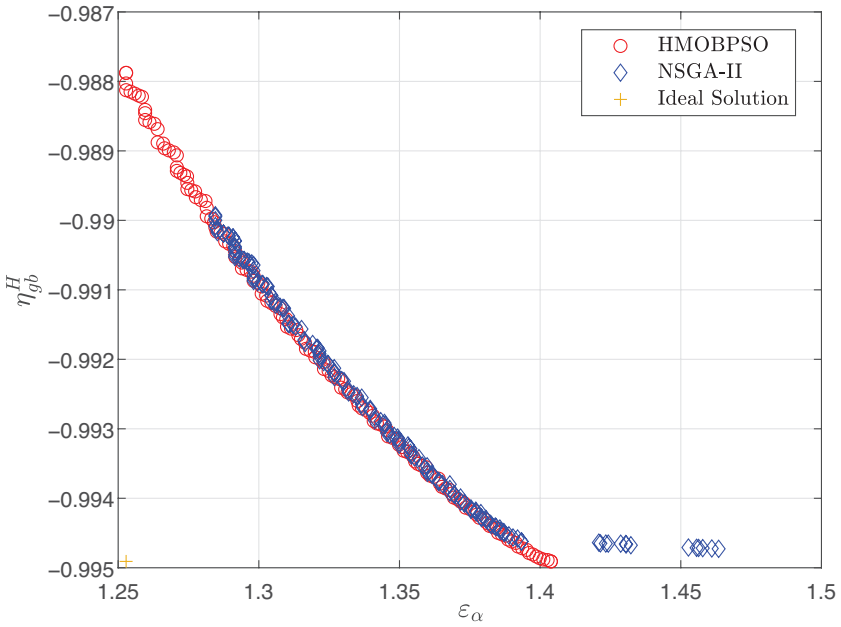

Figure 6. The appropriate Pareto-optimal curves obtained using the HMOBPSO and NSGA-II algorithms for the case where the contact ratio ε_α in combination with gearbox efficiency are taken as objectives.

Another important aspect for a gearbox is its safety and dimensions, which is analysed with the following combinations of objectives ε_α and σ_F, as well as ε_α and σ_H, where the appropriate Pareto-optimal curves are presented in Figure 7.

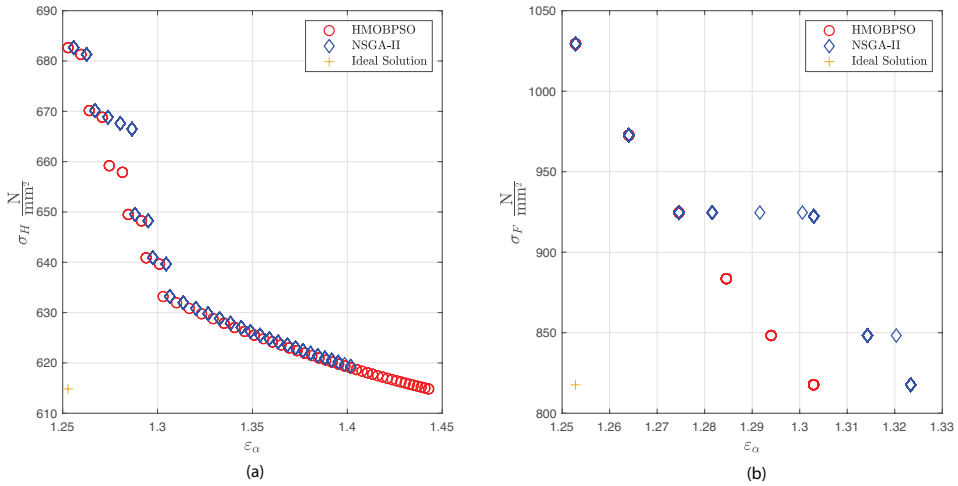

Figure 7. Pareto-optimal curves obtained using HMOBPSO and NSGA-II algorithms, for two combinations of objective functions (**a**) ε_α and σ_H and (**b**) ε_α and σ_F.

As in the previous case, we observe from Figure 7 that the considered paired objectives are conflicting, as the reduction in gearbox dimensions inevitably leads to the increase in appropriate stress. In the case of combination ε_α and σ_F , the ideal solution is 1.25 for the contact ratio and 924.6 N/mm^2 for the bending stress. In this regard, the compromise solution for this case is represented as a tuple $(\varepsilon_\alpha, \sigma_F)$ and is $(1.27, 817.7)$, which is obtained using the HMOBPSO algorithm, and $(1.27, 924.7)$ for the NSGA-II algorithm. For the combination of objectives ε_α and σ_H, the ideal solution is represented as a tuple $(\varepsilon_\alpha, \sigma_H)$ and is $(1.25, 614.8)$. The compromise solution obtained using the proposed algorithm is $(1.29, 634)$, while for the NSGA-II, it is $(1.4, 632)$.

By analyzing the three-dimensional Pareto-optimal curves for objectives such as contact ratio ε_α, gearbox efficiency η_{gb}^H, and gear strength (σ_F and σ_H), engineers can gain valuable insights into the trade-offs between these objectives. These insights can inform decision making and help engineers make more informed choices based on their priorities. For example, if the contact ratio is of utmost importance, the design engineer can identify the region on the Pareto curve that maximizes this objective while still considering the trade-offs with gearbox efficiency and strength. To enhance the evaluation of algorithmic performance in addressing the planetary gearbox MOO problem within a three-dimensional context, this study utilizes the Spacing metric. This metric is employed to assess the spread or diversity of solutions across the Pareto front, particularly when the problem's complexity is less apparent compared to a two-dimensional scenario. This metric is defined as

$$S = \sqrt{\frac{1}{n-1}\sum_{i=1}^{n}\left(\overline{d} - d_i\right)^2}, \tag{44}$$

where n is the number of non-dominated solutions, d_i is the Euclidean distance between the ith non-dominated vector and its nearest vectors in the Pareto set, and $\overline{d}$ is the mean of all d_i. A higher spacing metric value indicates a more evenly distributed set of solutions.

Therefore, the appropriate three-dimensional Pareto-optimal curves, for the case when three objectives have been considered, are depicted in Figure 8, where, for the objectives, the contact ratio ε_α, gearbox efficiency η_{gb}^H, and contact stress σ_H have been taken into the account.

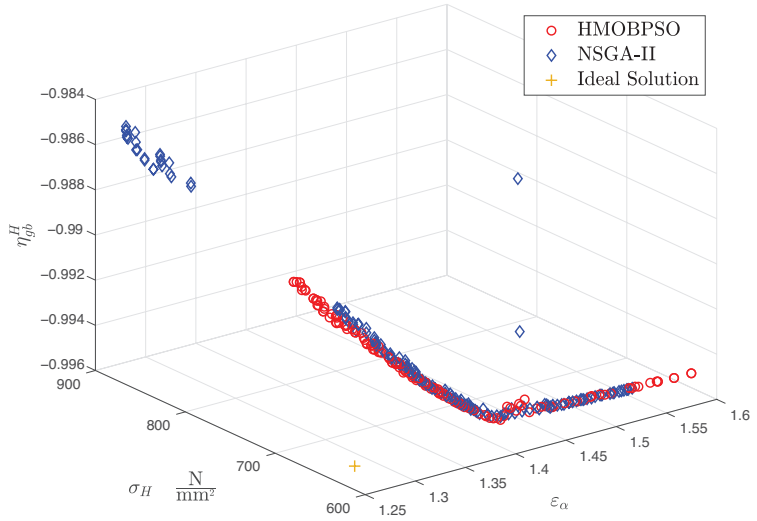

Figure 8. Three-dimensional Pareto-optimal curves obtained using the considered algorithms for the case with three objective functions, including ε_α, σ_H and η_{gb}^H.

From the results in Figure 8, we observe that all considered objectives are conflicting, where the increase in one objective leads to a decrease in the other two. In this regard, for comparison purposes, an ideal solution (which does not belong to the Pareto front but minimizes all objectives) is extracted as a tuple $\left(\varepsilon_\alpha, \sigma_H, \eta_{gb}^H\right) = (1.25, 614.8, 0.995)$, and the compromise solution obtained using the HMOBPSO algorithm is $(1.29, 633, 0.9925)$, and the solution obtained using NSGA-II is $(1.33, 630, 0.9903)$. The Spacing parameter of the NSGA-II algorithm is 3.25, while the proposed HMOBPSO achieved a higher spacing value of 4.99, showing that it is more efficient for the considered problem.

Next, we consider the following objectives: the contact ratio ε_α, gearbox efficiency η_{gb}^H, and root stress σ_F in the MOO problem, with the obtained Pareto curves displayed in Figure 9.

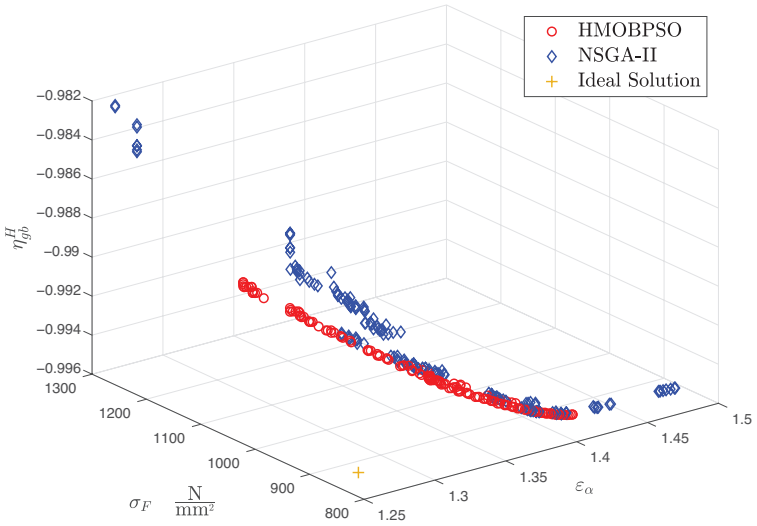

Figure 9. Three-dimensional Pareto-optimal curves obtained using the considered algorithms for the case with three objective functions, including ε_α, σ_F and η_{gb}^H .

From Figure 9, we can see that for the conflicting objectives, the ideal solution is a tuple $\left(\varepsilon_\alpha, \sigma_F, \eta_{gb}^H\right) = (1.25, 817.7, 0.9949)$, while the compromise solution obtained using the HMOBPSO algorithm is a tuple $(1.3, 860, 0.9912)$ and the solution given using the NSGA-II algorithm is $(1.31, 863, 0.9894)$. The spread indicator for the NSGA-II algorithm is

9.82, while for HMOBPSO, it is 17.77. This shows that the HMOBPSO is better suited for the considered optimization problem.

Upon examination of the data supplied in Table 5 and considering the findings from the Pareto-optimal fronts displayed in Figures 6–9, it is observed that in the majority of cases, the optimal solution is achieved using the HMOBPSO algorithm described in this paper. The best efficiency achieved is 0.9949, which is achieved with the proposed algorithm for the case of objectives ε_α and η_{gb}^H. In all other objective combinations, the best efficiency is achieved using the HMOBPSO algorithm. When compared to the industrial gearbox reference, the proposed approach demonstrates a notable enhancement in various aspects. Specifically, it yields a 35% decrease in gearbox volume and a 27.5% reduction in center distance, which directly corresponds to gearbox size, and a 2.56% gain in gearbox efficiency. By analyzing the Pareto fronts on Figures 6–9, we can see that the NSGA-II is not always able to obtain the whole Pareto-optimal set. Comparing the spacing values obtained in 3D Pareto fronts, we can see that the proposed algorithm is able to achieve higher spacing, which is more appropriate for complex design processes. Overall, the results show that the proposed algorithm offers significant improvements in terms of gearbox size, efficiency, and spacing compared to the NSGA-II. The reduction in gearbox volume and center distance not only reduces the overall size of the gearbox but also contributes to improved efficiency. Additionally, the higher spacing achieved using the proposed algorithm indicates that it is better suited to complex design processes, making it a more reliable and effective solution.

4.2. The Benchmark Results

In order to validate the performance in solving complex multi-objective optimization problems with the proposed modified HMOBPSO algorithm, a set of DTLZ and ZDT benchmark problems is employed in this paper. The ZDT benchmark problems were first introduced by Zitzler, Deb, and Thiele and have since become a standard test suite for multi-objective optimization algorithms [37]. The DTLZ problems are another popular set of benchmark problems for multi-objective optimization, which were introduced by Deb, Thiele, Laumanns, and Zitzler [38]. The solutions to these problems are known, making it possible to compare the performance of different algorithms. Therefore, these benchmark problems are widely used in the literature to evaluate the effectiveness of multi-objective optimization algorithms. The performance of the algorithm is evaluated based on its ability to find a set of Pareto-optimal solutions that provide a trade-off between the conflicting objectives. The proposed modified HMOBPSO algorithm is compared with other state-of-the-art multi-objective optimization algorithms, such as NSGA-II [16], MOPSO [33], CMOPSO [34], and MOBOA [35], on the ZDT and DTLZ benchmark problems to demonstrate its effectiveness.

To compare the optimization performance among the tested algorithms, the Inverted Generational Distance (IGD) is employed as the commonly used metric for evaluating the quality of a set of solutions obtained using a multi-objective optimization algorithm [39]. It measures the distance between the obtained solutions and the true Pareto-optimal front. The lower the IGD value, the better the quality of the solutions obtained. In addition to IDG, other performance metrics such as the hypervolume and spread are also used in the literature [39,40]. The IGD value is calculated using the following expression:

$$IGD = \frac{\sum_{v_i \in P_A} d(v_i, P_A)}{|P^*|}, \tag{45}$$

where $d(\cdot)$ represents the smallest possible Euclidean distance between v_i and the non-dominated solution set's points P_A, which are provided by the tested algorithm, P^* is a set of uniformly distributed points along the true Pareto-optimal front, and $|\cdot|$ denotes the operator that returns the number of the elements in the set. Ten thousand reference points were chosen at random from the resulting Pareto fronts to construct IGD metrics.

A Comparative Analysis of Statistical Performance

The Wilcoxon Signed-Rank and Friedman tests are commonly used statistical tests to compare the performance of different algorithms based on their IGD values [41]. The Wilcoxon Signed-Rank test is a non-parametric test used to compare two related samples, while the Friedman test is a non-parametric test used to compare more than two related samples. Since both of these tests are non-parametric tests, they do not require assumptions regarding the distribution of the data. These tests help to determine if there is a statistically significant difference between the algorithms' performances or if they perform similarly. Overall, the use of performance metrics and statistical tests is essential in determining the effectiveness of multi-objective optimization algorithms and selecting the most suitable algorithm for a given problem. In order to carry out statistical analysis in this paper, the experiments were conducted independently for a total of 30 iterations, and the standard deviation of the aforementioned performance metrics was computed. The statistical tests were performed with a significance level of $\alpha = 0.05$.

The Wilcoxon signed-rank test was applied in order to compare the performance of the two algorithms and reveal if the first algorithm taken for comparison outperforms the second method statistically. The present notation designates the summation of ranks for the scenario in which the first algorithm exhibits superior performance compared to the second as R^+, whereas the summation of ranks for the scenario in which the second algorithm outperforms the first is represented by R^-. In this regard, the null hypothesis of the Wilcoxon signed-rank test states that "it is assumed that there is no significant difference between the performance of the two algorithms" [41], and the alternative hypothesis states that there is a significant difference between the performance of the two tested algorithms. If the tested p-value is less than the significance α, then the null hypothesis is rejected. On the other hand, if the p-value is greater than α, the null hypothesis is accepted, and it can be concluded that there is no significant difference between the performance of the two algorithms.

The Friedman test, on the other hand, is used to compare the performance of more than two related samples and determine if there is a significant difference between them. Here, the algorithm that possesses the minimum rank value is identified as the most effective algorithm, whereas the algorithm with the highest rank is deemed to be the least effective algorithm. Therefore, the null hypothesis of the Friedman test is that there is "no significant difference between the performances of the tested algorithms" [41], and the alternative hypothesis is that "there is a significant difference between the performance of tested algorithms". The Friedman test uses the test statistic Q, which is calculated as the sum of squared deviations of the ranks of each algorithm from their mean rank, divided by a constant factor. The p-value obtained from the test is compared to the significance level α to determine if the null hypothesis should be rejected or not.

Table 6 presents the outcomes of numerical simulation conducted across 30 independent runs for each of the ZDT test problems under consideration. The results are presented in the form of mean and standard deviation values of IGD metrics.

From the results presented in Table 6, it is observed that the HMOBPSO algorithm showed the best performance on a number of considered problems, including DTLZ1, DTLZ3, DTLZ5, DTLZ6, and DTLZ7, while on other it had a performance similar to that of the best-performing algorithm. To achieve better insight into the obtained data presented in Table 6, the appropriate chart is created with the logarithm of the mean of IGD metric on the y-axis, which is depicted in Figure 10.

The Wilcoxon signed-rank test was used to undertake a statistical pair-wise comparison of the optimization performance of the proposed HMOBPSO and other examined algorithms. Table 7 displays the statistical results obtained from the application of Wilcoxon's signed-rank test on ZDT benchmark problems within the present context. The statistical analysis provided results that were used to assign one of three signs $(+, -, \approx)$ to the comparison of the algorithms. Regarding this matter, the symbol $(+)$ signifies that the initial algorithm exhibits a significantly superior performance compared to the second algo-

rithm, while the symbol $(-)$ indicates that the first algorithm's performance is significantly inferior to that of the second algorithm. The symbol $(\approx)$ denotes that the two algorithms being evaluated demonstrate comparable performance.

Table 6. The obtained mean and standard deviation values of the IGD metric for all used algorithms over all considered ZDT and DTLZ benchmark problems.

Test Instances	HMOBPSO	NSGA-II	MOBOA	CMOPSO	MOPSO
			Mean ± Std		
DTLZ1	2.5878×10^{-1} (2.78×10^{-1})	6.8853×10^{0} (1.77×10^{0})	2.1367×10^{0} (6.27×10^{0})	1.3832×10^{1} (4.54×10^{0})	4.3650×10^{0} (2.50×10^{0})
DTLZ2	6.9384×10^{-2} (2.53×10^{-3})	5.6932×10^{-2} (7.66×10^{-4})	3.5930×10^{-1} (2.92×10^{-2})	5.8342×10^{-2} (1.06×10^{-3})	1.2624×10^{-1} (2.13×10^{-2})
DTLZ3	7.6168×10^{0} (3.99×10^{0})	1.1711×10^{2} (1.57×10^{1})	3.2117×10^{2} (5.48×10^{1})	1.3933×10^{2} (3.99×10^{1})	1.3230×10^{2} (5.20×10^{1})
DTLZ4	1.4369×10^{-1} (1.99×10^{-1})	6.2684×10^{-2} (6.03×10^{-3})	8.8102×10^{-1} (1.13×10^{-1})	1.4057×10^{-1} (2.53×10^{-1})	3.0302×10^{-1} (2.65×10^{-1})
DTLZ5	6.0880×10^{-3} (3.45×10^{-4})	5.3969×10^{-2} (5.44×10^{-3})	2.6824×10^{-1} (3.37×10^{-2})	7.3418×10^{-3} (5.74×10^{-4})	9.1614×10^{-3} (1.39×10^{-3})
DTLZ6	1.0085×10^{-2} (5.19×10^{-2})	2.6649×10^{-1} (2.64×10^{-1})	7.8499×10^{0} (4.91×10^{-1})	1.5201×10^{-1} (4.00×10^{-1})	9.1875×10^{0} (1.11×10^{-1})
DTLZ7	1.0292×10^{-1} (5.36×10^{-2})	2.8526×10^{-1} (1.01×10^{-1})	6.7820×10^{0} (5.19×10^{-1})	1.4424×10^{-1} (1.85×10^{-1})	6.9118×10^{0} (7.16×10^{-1})
ZDT1	1.2544×10^{-2} (2.28×10^{-3})	2.4370×10^{-2} (1.62×10^{-2})	1.6425×10^{0} (1.30×10^{-1})	5.0456×10^{-3} (3.85×10^{-4})	1.6634×10^{0} (9.22×10^{-2})
ZDT2	2.7702×10^{-2} (4.03×10^{-2})	2.3539×10^{-2} (3.32×10^{-2})	2.5048×10^{0} (1.38×10^{-1})	4.6474×10^{-3} (3.57×10^{-4})	3.1771×10^{0} (2.18×10^{-1})

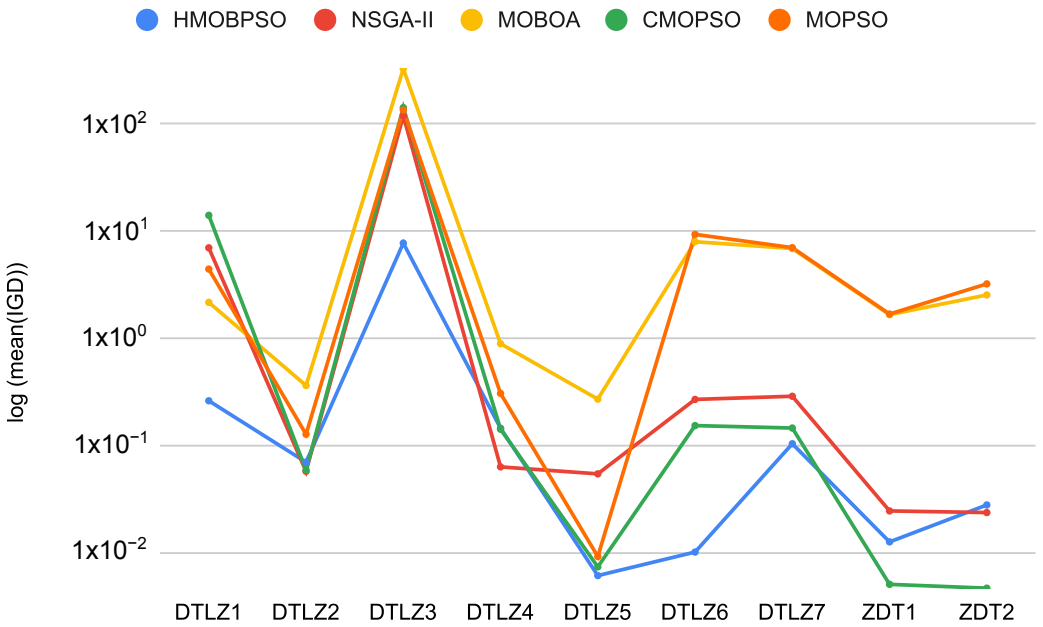

Figure 10. Visual representation of the mean of IGD metric from Table 6.

Table 7. The results of Wilcoxon's statistical test between the proposed HMOBPSO and the other algorithms taken for consideration on the selected ZDT and DTLZ benchmark problems.

Algorithms	R^+	R^-	p-Value	Dec.
HMOBPSO vs. NSGA-II	36	9	0.1289	$\approx$
HMOBPSO vs. MOBOA	45	0	0.0039	$+$
HMOBPSO vs. MOPSO	45	0	0.039	$+$
HMOBPSO vs. CMOPSO	31	14	0.3594	$\approx$

From the results in Table 7, it can be concluded that the proposed HMOBPSO algorithm achieved similar performance to the NSGA-II and CMOPSO algorithms, while still providing higher R^+ values than R^- in these cases. Compared to the MOBOA and MOPSO, it clearly outperformed these algorithms.

Table 8 displays the mean rankings of the analyzed algorithms for various objective functions of the ZDT benchmark problems, as per Friedman's methodology, which is performed to evaluate the efficiency of the proposed HMOBPSO algorithm with regard to other state-of-the-art multi-objective optimization algorithms taken for analysis.

Table 8. The results of the Friedman statistical test for all algorithms across all ZDT and DTLZ test problems, with a significance level of $\alpha = 0.05$.

Algorithm	DTLZ1	DTLZ2	DTLZ3	DTLZ4	DTLZ5	DTLZ6	DTLZ7	ZDT1	ZDT2	Mean Ranking	Rank
HMOBPSO	**1**	2.67	**1**	2.55	**2.22**	**1.667**	**1.78**	1.89	**1.89**	1.85	1
NSGA-II	3	2.55	2	**2.11**	3.11	1.889	2.33	**1.78**	2	2.35	2
CMOPSO	4	**2.22**	4	2.67	2.67	2.44	1.89	2.33	2.11	2.78	3
MOPSO	2	2.67	3	2.67	3	5	4.79	4.44	4.89	3.45	4
MOBOA	5	4.89	5	5	4	4	4.22	4.55	4.11	4.58	5
Friedman p value	0	0	0	0	0	0	0	0	0		

Here, we display in bold the rank of the best-performing algorithm for the considered problem, while the second-best algorithm is underlined. When analyzing the results in Table 8, we observe that the obtained p values are lower than the significance $\alpha = 0.05$, meaning that there exists a significant difference between the performance of algorithms taken for consideration. We observe that the HMOBPSO algorithm achieved the best overall rank, which is in agreement with the results of Wilcoxon's test. Hence, the statistical analysis of the outcomes validates the efficacy of the hybrid algorithm proposed in this paper.

5. Conclusions

The present paper examines the multi-objective optimization of the planetary gearbox, taking into account various objective functions, including the center distance, gear volume, gearbox efficiency, and the surface and bending stresses. A multi-objective optimization model was developed for a planetary gearbox, incorporating various objectives and several constraints, such as safety and reliability constraints, mounting constraints, and a constraint ensuring uniform wear of the tooth profile. This study presents a novel hybrid method, namely HMOBPSO, which integrates the PSO and BOA algorithms to address a challenging MOO problem. The proposed approach integrates the PSO velocity update scheme into the equations governing butterfly movement. Additionally, it combines the use of crowding distance to optimize the selection of individuals. Furthermore, it suggests the inclusion of an adaptive parameter for individual position updates and the substitution of switch probability.

The algorithm under consideration has successfully generated the non-convex Pareto frontier, which serves as a graphical representation of the interplay between opposing objectives and is of importance for the designer in facilitating the selection of suitable building parameters. The obtained findings were subjected to validation and subsequently compared with the parameters of the reference industrial gearbox. The analysis revealed a significant reduction in center distance, with a maximum decrease of 27.5%. Additionally, the volume of the gearbox exhibited a notable improvement of 35%. Furthermore, the efficiency of the gearbox displayed an enhancement of 2.56%. In addition, an assessment of the optimization performance of the HMOBPSO algorithm was conducted by comparing it to other established algorithms across several ZDT and DTLZ benchmark problems. The efficacy of the HMOBPSO algorithm in the optimization of the planetary gearbox model is evidenced by the improved solutions it yields in comparison to the NSGA-II method. This observation underscores the efficacy and resilience of the algorithm proposed for identifying optimal solutions.

Future work can focus on examining the algorithm's effectiveness across other issue domains and exploring its capacity for addressing more intricate optimization challenges.

Author Contributions: Conceptualization, Methodology and Validation, M.S. and M.R.; Formal Analysis, Software, Investigation, Data Curation, M.S. and M.R.; Resources, M.S.; Writing—Original Draft Preparation, M.S.; Writing—Review and Editing, M.S.; Visualization, M.S. and M.R.; Supervision, M.S. All authors have read and agreed to the published version of the manuscript.

Funding: The research of M. Sedak was supported by the Serbian Ministry of Education and Science under Grant No. TR35006. The research of M. Rosić was supported by the Serbian Ministry of Education and Science under Grant TR35029.

Institutional Review Board Statement: Not applicable.

Informed Consent Statement: Not applicable.

Data Availability Statement: No new data were created or analyzed in this study. Data sharing is not applicable to this article.

Conflicts of Interest: The authors declare no conflict of interest.

Nomenclature

K_A	Application factor (-)
a_{ag}	Center distance between sun and planet gears (mm)
Y_ε	Contact ratio factor (-)
Z_ε	Contact ratio factor (-)
K_v	Dynamic factor(-)
Z_E	Elasticity factor $(\sqrt{\mathrm{N/mm^2}})$
$K_{F\alpha}$	Face load factor (-)
$\mathbb{F}$	Feasible domain of the optimization problem
b	Gear width (mm)
β	Helix angle $(^\circ)$
Z_N	Life factor for contact stress (-)
Z_L	Lubricant factor (-)
m_n	Module (mm)
E	Modulus of elasticity of gears $(\mathrm{kN/mm^2})$
α_n	Normal pressure angle $(^\circ)$
n_w	Number of planet gears (-)
z_g	Number of teeth of planet gear (-)
z_b	Number of teeth of ring gear (-)
z_a	Number of teeth of sun gear (-)
$d_{a(g)}$	Outside diameter of planet gear (mm)
$d_{a(b)}$	Outside diameter of ring gear (mm)
$d_{a(a)}$	Outside diameter of sun gear (mm)
d_s	Outside bearing diameter (mm)
D	Outside diameter of ring gear (mm)
η_{gb}^H	Planetary gearbox efficiency (-)
x_g	Profile shift coefficient of planet gear (-)
x_b	Profile shift coefficient of ring gear (-)
x_a	Profile shift coefficient of sun gear (-)
$d_(a)$	Pitch circle of sun gear (mm)
$d_(g)$	Pitch circle of planet gear (mm)
Y_{RelT}	Relative surface factor (-)
Z_R	Roughness factor affecting surface durability (-)
Y_{ST}	Stress concentration factor (-)
Y_{Sa}	Stress correction factor (-)
Y_{Fa}	Tooth form factor (-)
F_t	Transverse component of the normal force (N)

$K_{H\alpha}$	Transverse load factor (-)
α_t	Transverse pressure angle ($^\circ$)
V	Volume of gears (mm^3)
Z_H	Zone factor (-)

Appendix A

The values and procedures for the calculation of different factors used in the calculation of the contact and bending stress of the planetary gearbox are outlined in this section. The contact ratio factors Y_ε and Z_ε, as well as zone factor Z_H, are determined according to the expressions in [42,43]. The factors Y_{Fa} and Y_{Sa} are calculated according to the DIN3990 standard method C [42]. The values of the application factor and elasticity factor are taken as $K_A = 1.2$ and $Z_E = 189.9\sqrt{N/mm^2}$, respectively. Dynamic factor K_v and face and transverse load factors $K_{F\alpha}$ and $K_{H\alpha}$ are calculated according to method B and method C of the ISO standard, respectively [43]. Furthermore, the relative surface factor Y_{RelT}, stress concentration factor Y_{ST}, life factor for contact stress Z_N, lubricant factor Z_L, and roughness factor affecting surfaces Z_R are determined according to [42,43].

References

1. Nutakor, C.; Kłodowski, A.; Sopanen, J.; Mikkola, A.; Pedrero, J.I. Planetary gear sets power loss modeling: Application to wind turbines. *Tribol. Int.* **2017**, *105*, 42–54. [CrossRef]
2. Xu, X.; Chen, J.; Lin, Z.; Qiao, Y.; Chen, X.; Zhang, Y.; Xu, Y.; Li, Y. Optimization design for the planetary gear train of an electric vehicle under uncertainties. *Actuators* **2022**, *11*, 49. [CrossRef]
3. Mao, Y.; Niu, S.; Yang, Y. Differential Evolution Based Multi-Objective Optimization of the Electrical Continuously Variable Transmission System. *IEEE Trans. Ind. Electron.* **2017**, *65*, 2080–2089. [CrossRef]
4. Sedak, M.; Rosić, B. Multi-objective optimization of planetary gearbox with adaptive hybrid particle swarm differential evolution algorithm. *Appl. Sci.* **2021**, *11*, 1107. [CrossRef]
5. Xu, H.; Kahraman, A.; Anderson, N.; Maddock, D. Prediction of mechanical efficiency of parallel-axis gear pairs. *J. Mech. Des.* **2007**, *129*, 58–68. [CrossRef]
6. Marques, P.M.; Camacho, R.; Martins, R.C.; Seabra, J.H. Efficiency of a planetary multiplier gearbox: Influence of operating conditions and gear oil formulation. *Tribol. Int.* **2015**, *92*, 272–280. [CrossRef]
7. Liu, H.; Liu, H.; Zhu, C.; Parker, R.G. Effects of lubrication on gear performance: A review. *Mech. Mach. Theory* **2020**, *145*, 103701. [CrossRef]
8. Miler, D.; Lončar, A.; Žeželj, D.; Domitran, Z. Influence of profile shift on the spur gear pair optimization. *Mech. Mach. Theory* **2017**, *117*, 189–197. [CrossRef]
9. Abderazek, H.; Ferhat, D.; Ivana, A. Adaptive mixed differential evolution algorithm for bi-objective tooth profile spur gear optimization. *Int. J. Adv. Manuf. Technol.* **2017**, *90*, 2063–2073. [CrossRef]
10. Abderazek, H.; Sait, S.M.; Yildiz, A.R. Optimal design of planetary gear train for automotive transmissions using advanced meta-heuristics. *Int. J. Veh. Des.* **2019**, *80*, 121–136. [CrossRef]
11. Yaw, M.; Chong, K. Optimize Volume for Planetary Gear Train by using Algorithm Based Artificial Immune System. *Int. J. Adv. Trends Comput. Sci. Eng.* **2020**, *9*, 3. [CrossRef]
12. Kahouli, O.; Alsaif, H.; Bouteraa, Y.; Ben Ali, N.; Chaabene, M. Power system reconfiguration in distribution network for improving reliability using genetic algorithm and particle swarm optimization. *Appl. Sci.* **2021**, *11*, 3092. [CrossRef]
13. Rosić, M.; Sedak, M.; Simić, M.; Pejović, P. An Improved Chaos Driven Hybrid Differential Evolutionand Butterfly Optimization Algorithm for Passive Target Localization Using TDOA Measurements. *Appl. Sci.* **2023**, *13*, 684. [CrossRef]
14. Kennedy', J.; Eberhart, R. Particle Swarm Optimization. In Proceedings of the ICNN'95-International Conference on Neural Networks, Perth, Australia, 27 November–1 December 1995; p. 7.
15. Arora, S.; Singh, S. Butterfly optimization algorithm: A novel approach for global optimization. *Soft Comput.* **2019**, *23*, 715–734. [CrossRef]
16. Deb, K.; Pratap, A.; Agarwal, S.; Meyarivan, T. A fast and elitist multiobjective genetic algorithm: NSGA-II. *IEEE Trans. Evol. Comput.* **2002**, *6*, 182–197. [CrossRef]
17. Robič, T.; Filipič, B. DEMO: Differential Evolution for Multiobjective Optimization. In *Evolutionary Multi-Criterion Optimization*; Series Title: Lecture Notes in Computer Science; Hutchison, D., Kanade, T., Kittler, J., Kleinberg, J.M., Mattern, F., Mitchell, J.C., Naor, M., Nierstrasz, O., Pandu Rangan, C., Steffen, B., et al., Eds.; Springer: Berlin/Heidelberg, Germany, 2005; Volume 3410, pp. 520–533. [CrossRef]
18. Sharma, S.; Khodadadi, N.; Saha, A.K.; Gharehchopogh, F.S.; Mirjalili, S. Non-dominated sorting advanced butterfly optimization algorithm for multi-objective problems. *J. Bionic Eng.* **2023**, *20*, 819–843. [CrossRef]
19. Cui, Y.; Geng, Z.; Zhu, Q.; Han, Y. Multi-objective optimization methods and application in energy saving. *Energy* **2017**, *125*, 681–704. [CrossRef]

20. Rangaiah, G.P.; Feng, Z.; Hoadley, A.F. Multi-objective optimization applications in chemical process engineering: Tutorial and review. *Processes* **2020**, *8*, 508. [CrossRef]
21. Belarhzal, S.; Daoudi, K.; Boudi, E.M.; Bachir, A.; Elmoumen, S. A multiobjective optimization analysis of spur gear pair: The profile shift factor effect on structure design and efficiency. *Math. Probl. Eng.* **2021**, *2021*, 8873769. [CrossRef]
22. Patil, M.; Ramkumar, P.; Shankar, K. Multi-objective optimization of the two-stage helical gearbox with tribological constraints. *Mech. Mach. Theory* **2019**, *138*, 38–57. [CrossRef]
23. Parmar, A.; Ramkumar, P.; Shankar, K. Macro geometry multi-objective optimization of planetary gearbox considering scuffing constraint. *Mech. Mach. Theory* **2020**, *154*, 104045. [CrossRef]
24. Maputi, E.S.; Arora, R. Multi-objective optimization of a 2-stage spur gearbox using NSGA-II and decision-making methods. *J. Braz. Soc. Mech. Sci. Eng.* **2020**, *42*, 477. [CrossRef]
25. Wang, C. Multi-objective optimal design of modification for helical gear. *Mech. Syst. Signal Process.* **2021**, *157*, 107762. [CrossRef]
26. Artoni, A. A methodology for simulation-based, multiobjective gear design optimization. *Mech. Mach. Theory* **2019**, *133*, 95–111. [CrossRef]
27. Yao, Q. Multi-objective optimization design of spur gear based on NSGA-II and decision making. *Adv. Mech. Eng.* **2019**, *11*, 1687814018824936. [CrossRef]
28. Lei, Y.; Hou, L.; Fu, Y.; Hu, J.; Chen, W. Research on vibration and noise reduction of electric bus gearbox based on multi-objective optimization. *Appl. Acoust.* **2020**, *158*, 107037. [CrossRef]
29. Dixit, Y.; Kulkarni, M.S. Multi-Objective Optimization with Solution Ranking for Design of Spur Gear Pair Considering Multiple Failure Modes. *Tribol. Int.* **2023**, *180*, 108284. [CrossRef]
30. Miler, D.; Žeželj, D.; Lončar, A.; Vučković, K. Multi-objective spur gear pair optimization focused on volume and efficiency. *Mech. Mach. Theory* **2018**, *125*, 185–195. [CrossRef]
31. Liu, J.; Zhang, H.; He, K.; Jiang, S. Multi-objective particle swarm optimization algorithm based on objective space division for the unequal-area facility layout problem. *Expert Syst. Appl.* **2018**, *102*, 179–192. [CrossRef]
32. Yue, C.; Qu, B.; Liang, J. A Multi-objective Particle Swarm Optimizer Using Ring Topology for Solving Multimodal Multi-objective Problems. *IEEE Trans. Evol. Comput.* **2017**, *22*, 805–817. [CrossRef]
33. Raquel, C.R.; Naval, P.C., Jr. An effective use of crowding distance in multiobjective particle swarm optimization. In Proceedings of the 7th Annual Conference on Genetic and Evolutionary Computation, Washington, DC, USA, 25–29 June 2005; pp. 257–264.
34. Zhang, X.; Zheng, X.; Cheng, R.; Qiu, J.; Jin, Y. A competitive mechanism based multi-objective particle swarm optimizer with fast convergence. *Inf. Sci.* **2018**, *427*, 63–76. [CrossRef]
35. Ahmed, M.M.; Hassanien, A.E.; Tang, M. Multi-objective butterfly optimization algorithm for solving constrained optimization problems. In *LISS 2021: Proceedings of the 11th International Conference on Logistics, Informatics and Service Sciences*; Springer: Berlin/Heidelberg, Germany, 2022; pp. 389–400.
36. *Design Manual for Enclosed Epicyclic Gear Drives*; American Gear Manufacturers Association: Alexandria, VA, USA, 2016.
37. Zitzler, E.; Deb, K.; Thiele, L. Comparison of multiobjective evolutionary algorithms: Empirical results. *Evol. Comput.* **2000**, *8*, 173–195. [CrossRef] [PubMed]
38. Deb, K.; Thiele, L.; Laumanns, M.; Zitzler, E. *Scalable Test Problems for Evolutionary Multiobjective Optimization*; Springer: Berlin/Heidelberg, Germany, 2005.
39. Yu, X. Differential evolution mutation operators for constrained multi-objective optimization. *Appl. Soft Comput.* **2018**, *67*, 452–466. [CrossRef]
40. Zhang, Q.; Zhou, A.; Zhao, S.; Suganthan, P.N.; Liu, W.; Tiwari, S. Multiobjective Optimization Test Instances for the CEC 2009 Special Session and Competition. 2009; p. 30. Available online: https://www.al-roomi.org/multimedia/CEC_Database/CEC2009/MultiObjectiveEA/CEC2009_MultiObjectiveEA_TechnicalReport.pdf (accessed on 10 June 2023).
41. Derrac, J.; García, S.; Molina, D.; Herrera, F. A practical tutorial on the use of nonparametric statistical tests as a methodology for comparing evolutionary and swarm intelligence algorithms. *Swarm Evol. Comput.* **2011**, *1*, 3–18. [CrossRef]
42. *Calculation of Load Capacity of Cylindrical Gears*; German Institute for Standardization—DIN: Berlin, Germany, 1987.
43. *Calculation of Load Capacity of Spur and Helical Gears*; International Organization for Standardization: Geneva, Switzerland, 1996.

Disclaimer/Publisher's Note: The statements, opinions and data contained in all publications are solely those of the individual author(s) and contributor(s) and not of MDPI and/or the editor(s). MDPI and/or the editor(s) disclaim responsibility for any injury to people or property resulting from any ideas, methods, instructions or products referred to in the content.